Developmental Biology 341 (2010) 400–415

Contents lists available at ScienceDirect

Developmental Biology

journal homepage: www.elsevier.com/developmentalbiology

UDP xylose synthase 1 is required for morphogenesis and histogenesis of the craniofacial skeleton

B. Frank Eames [a,1], Amy Singer [a,1], Gabriel A. Smith [a,e,1], Zachary A. Wood [b,c], Yi-Lin Yan [a], Xinjun He [a], Samuel J. Polizzi [c], Julian M. Catchen [a], Adriana Rodriguez-Mari [a], Tor Linbo [d], David W. Raible [d], John H. Postlethwait [a,*]

[a] Institute of Neuroscience, 1254 University of Oregon, Eugene OR 97403-1254, USA
[b] Institute of Molecular Biology, University of Oregon, Eugene OR 97403, USA
[c] Department of Biochemistry & Molecular Biology, University of Georgia, 120 Green Street, Athens, GA 30602, USA
[d] Department of Biological Structure, University of Washington, Seattle, WA 98195-7420, USA
[e] Temple University, School of Medicine, 3420 North Broad Street, Philadelphia, PA 19140, USA

ARTICLE INFO

Article history:
Received for publication 3 October 2009
Revised 13 February 2010
Accepted 24 February 2010
Available online 11 March 2010

Keywords:
Extracellular matrix
Zebrafish
Skeletogenesis
Cartilage
Perichondrium
Glycosaminoglycans
Heparan sulfate
Chondroitin sulfate
Proteoglycans
Hedgehog signaling
Neural crest
UDP-xylose synthase
FGF signaling

ABSTRACT

UDP-xylose synthase (Uxs1) is strongly conserved from bacteria to humans, but because no mutation has been studied in any animal, we do not understand its roles in development. Furthermore, no crystal structure has been published. Uxs1 synthesizes UDP-xylose, which initiates glycosaminoglycan attachment to a protein core during proteoglycan formation. Crystal structure and biochemical analyses revealed that an R233H substitution mutation in zebrafish *uxs1* alters an arginine buried in the dimer interface, thereby destabilizing and, as enzyme assays show, inactivating the enzyme. Homozygous *uxs1* mutants lack Alcian blue-positive, proteoglycan-rich extracellular matrix in cartilages of the neurocranium, pharyngeal arches, and pectoral girdle. Transcripts for *uxs1* localize to skeletal domains at hatching. GFP-labeled neural crest cells revealed defective organization and morphogenesis of chondrocytes, perichondrium, and bone in *uxs1* mutants. Proteoglycans were dramatically reduced and defectively localized in *uxs1* mutants. Although *col2a1a* transcripts over-accumulated in *uxs1* mutants, diminished quantities of Col2a1 protein suggested a role for proteoglycans in collagen secretion or localization. Expression of *col10a1, indian hedgehog*, and *patched* was disrupted in mutants, reflecting improper chondrocyte/perichondrium signaling. Up-regulation of *sox9a, sox9b,* and *runx2b* in mutants suggested a molecular mechanism consistent with a role for proteoglycans in regulating skeletal cell fate. Together, our data reveal time-dependent changes to gene expression in *uxs1* mutants that support a signaling role for proteoglycans during at least two distinct phases of skeletal development. These investigations are the first to examine the effect of mutation on the structure and function of Uxs1 protein in any vertebrate embryos, and reveal that Uxs1 activity is essential for the production and organization of skeletal extracellular matrix, with consequent effects on cartilage, perichondral, and bone morphogenesis.

Introduction

The vertebrate skeleton provides structural support for muscle attachments and a protective casing for vulnerable internal organs. These functions rely on the coordinated secretion of dense extracellular matrix (ECM) by skeletal precursor cells during embryonic development. Proteinaceous components of skeletal ECM include collagens, elastin, and proteoglycans. Collagens anchor and reinforce the ECM; elastin provides flexibility (Velleman, 2000); and proteoglycans impact cell division, cell adhesion, and migration (Holt and Dickson, 2005; Kirn-Safran et al., 2004; Lander and Selleck, 2000; Knudson and Knudson, 2001). Proteoglycans contain repeating disaccharides (glycosaminoglycans, or GAGs) linked to a protein core (Prydz and Dalen, 2000) and include four major classes: dermatan, keratan, chondroitin, and heparan sulfate. In addition to imparting hydrostatic properties to skeletal tissues through GAG sulfation and hydration, proteoglycans can play a role in cell signaling. For example, heparan sulfate proteoglycans (HSPGs) help cell receptors bind growth factors (Izvolsky et al., 2003; Lin et al., 1999) and although the mechanism remains unclear, *Cspg1* (*Aggrecan*)-deficient mutant chickens have dwarfed bones (Velleman and Clark, 1992).

* Corresponding author. Fax: +1 541 346 4548.
E-mail addresses: bfeame@uoneuro.uoregon.edu (B.F. Eames), asinger@zfin.org (A. Singer), gabe.smith@temple.edu (G.A. Smith), zac@bmb.uga.edu (Z.A. Wood), yan@uoneuro.uoregon.edu (Y.-L. Yan), xhe@uoneuro.uoregon.edu (X. He), spolizzi@uga.edu (S.J. Polizzi), catchen@cs.uoregon.edu (J.M. Catchen), arodrig4@uoregon.edu (A. Rodriguez-Mari), tlinbo@u.washington.edu (T. Linbo), draible@u.washington.edu (D.W. Raible), jpostle@uoneuro.uoregon.edu (J.H. Postlethwait).
[1] These authors contributed equally to the work.

0012-1606/$ – see front matter © 2010 Elsevier Inc. All rights reserved.
doi:10.1016/j.ydbio.2010.02.035

Not all bones are created equal. Dermal bones differentiate osteoblasts directly via intramembranous ossification, but chondral bones form by endochondral ossification, during which developing chondrocytes and an overlying osteogenic epithelium, the perichondrium, interact (Eames et al., 2003). Understanding how these cell types signal each other and how proteoglycans play structural roles is important because impaired signaling between chondrocytes and osteoprogenitors can lead to osteoarthritis, a disease in which bone spurs replace cartilage in many people over age 65 (Ala-Kokko et al., 1990; Kizawa et al., 2005; Knowlton et al., 1990; Rothschild and Panza, 2007).

Proteoglycan biosynthesis initiates with the addition of a common tetrasaccharide linker to a core protein. Vertebrates use UDP-xylose, the first sugar in the linker, almost exclusively for proteoglycan synthesis (xylose is also added to EGF-repeat domains of some proteins (Bakker et al., 2009; Ishimizu et al., 2007). UDP-xylose biosynthesis begins with the conversion of UDP-glucose into UDP-glucuronic acid by UDP-glucose dehydrogenase (Ugdh). Zebrafish with diminished Ugdh activity have defective craniofacial and coronary development (Neuhauss et al., 1996; Walsh and Stainier, 2001). Next, UDP-xylose synthase (Uxs1, also called UDP-glucuronic acid decarboxylase or UGD, EC 4.1.1.35) converts UDP-glucuronic acid into UDP-xylose (Kearns et al., 1993; Vertel et al., 1993). The GAG tetrasaccharide linker of proteoglycans is initiated by a xylosyltransferase, which adds UDP-xylose to a serine residue of the core protein. Galactose and glucuronic acid transferases then add two galactoses and one glucuronic acid, completing the tetrasaccharide linker. GAG synthesis continues as exostosins (Ext1a, Ext1b, Ext1c, Ext2, Extl2, and Extl3 in zebrafish) add disaccharide constituents (Kjellen and Lindahl, 1991; Knudson and Knudson, 2001; Lin, 2004). Zebrafish mutations in *ext2* (*dackel* (*dak*)), *extl3* (*boxer* (*box*)), and *solute carrier family 35, member b2* (*pinscher* (*pic*); previously termed *3'-phosphoadenosine 5'-phosphosulfate transporter 1*, or *papst1*) show that GAG synthesis and sulfation are important for axon sorting and cartilage morphogenesis (Clement et al., 2008; Lee et al., 2004; Schilling et al., 1996). The developmental roles of Uxs1, however, are poorly understood because vertebrate models that lack Uxs1 activity have not yet been investigated.

In a mutation screen for neural crest defects, we identified *man o'war* (*mow*), which, like the *sox9a* mutation *jellyfish* (Yan et al., 2002), fails to form craniofacial cartilages. Our molecular genetic analyses showed that the *mow*^{w60} mutation causes an amino acid replacement in the zebrafish *uxs1* gene and is allelic to the viral insert *hi3357* (Amsterdam et al., 2004; Golling et al., 2002; Nissen et al., 2006). Sequence alignments reveal Uxs1 to be one of the most highly conserved non-mitochondrial proteins, preserving 57% amino acid identity between the bacterium *Rhodospirillum rubrum* and human. Using the crystal structure of human UXS1, we modeled the *mow*^{w60} substitution and found it to disrupt interactions at the enzyme's dimer interface, which should reduce or eliminate enzymatic activity. Indeed, our biochemical analyses revealed that an amino acid replacement homologous to the *mow*^{w60} allele destroys human UXS1 activity. Transcripts of *uxs1* are deposited maternally, and then *uxs1* is expressed zygotically in regions of the developing craniofacial skeleton. Histochemical and immunohistochemical investigations showed that wild-type *uxs1* is essential for the production and organization of many components of the ECM, including both proteoglycans and collagens. Additionally, confocal microscopy of GFP-labeled cranial neural crest cells revealed a critical role for *uxs1* in directing the morphology of chondrocytes, perichondrium, and bone during craniofacial development. Our molecular analyses demonstrated that chondrocyte maturation and Hedgehog signaling is dependent upon *uxs1*. Finally, our observation that the early chondrogenic markers *sox9a, sox9b,* and *runx2b* were up-regulated in *uxs1* mutants provide a mechanistic explanation for many of the defects in endochondral ossification, and furthermore suggest a novel feedback role for proteoglycans as skeletal progenitor cells undergo differentiation. Specifically, our data show proteoglycans to modify signaling pathways in early chondrogenic condensations and in later interactions between chondrocytes and perichondrium.

Materials and methods

Mapping and cloning of mow^{w60}

Adult male AB zebrafish (*Danio rerio*) were treated with ethylnitrosourea to induce point mutations and out-crossed to wild-type females. F2 families were produced and F3 larvae were screened for mutant phenotypes. The *mow*^{w60} allele showed reduced pharyngeal cartilages. For mapping, heterozygous *mow*^{w60} fish on an AB background were mated to WIK wild-type fish. F2 individuals were genotyped for 311 well-distributed simple sequence repeats (Knapik et al., 1998; Shimoda et al., 1999), identifying linked zmarker z3124. The zebrafish genome sequence nearby was screened for candidate genes involved in skeletal differentiation and mapping primers were designed in candidate genes. For *uxs1,* primers were designed to amplify a simple sequence repeat (SSR) in intron-7 (scaff346.117 + GCAGCGTGAAAAAGCAAAGAC and scaff346.524-ACCGCCGC-CTGTGACGA). cDNA for *uxs1* was amplified and isolated for sequencing using overlapping fragments amplified by primer sets designed from NM_173242 (Uxs1.114 + TGACCGTTGGACAAGGGAGGATTTA, Uxs1.421-CTATTTGAAGAGCGGCTGCACGACTAT; Uxs1.309 + AGCCGAAAA-TAAACTGCCCAGACTACTT, Uxs1.594-CATCCGCATCATCCTCCAGCACAC; Uxs1.394 + CATAGTCGTGCAGCCGCTCTTCAAAT, Uxs1.757-GTCCCACTGCCTCATCTATCCTCTGCTC; Uxs1.854 + TCACCGGTGGGGCAG-GATTC, Uxs1.1397-ACCACTCGCCCGTCGTTCAT; Uxs1.945 + CGGCCGCAAGCGCAATGTAGA, Uxs1.1340-ACTCGCACCTCCA-CTCCTTCCTGTTTC; Uxs1.1251 + TGGTCCCCGGGCCTGTTATGATG, Uxs1.1685-AGTTTGGCCCTGCGGATGTCG). To genotype *mow*^{w60} fish, we used primers MOW.928 + CACCCCCAAAATGAGGACTACTG and MOW.1277-AGAGCTCGCAACGGCATAAGAT, which amplify a 349 bp fragment that yields 274 and 75 bp fragments from the *mow*^{w60} mutant amplicon but leaves the wild-type amplicon intact after digestion by *NspI*. To detect the *hi3357* pro-viral insertion, we used primers that flank the insertion site (Uxs1.e1.398 + GTCGTGCAGCCGCTCTTCAAAT and Uxs1.e1.597-GCTCATCCGCATCATCCTCCAG) and yield a 199 bp fragment from wild type but no fragment from homozygous *hi3357* mutants; a *wnt5a* amplicon verified DNA quality (Golling et al., 2002). All work with animals was approved by the appropriate Institutional Animal Care and Use Committee.

Sequence alignments

Uxs1 sequences: human, *Homo sapiens* NP_079352 (179/311, 57% identity to the bacterial protein); mouse, *Mus musculus* NP_080706 (179/311, 57%); chicken *Gallus gallus* XP_416926 (180/311, 57%); frog *Xenopus tropicalis* NP_001006849 (178/311, 57%); pufferfish *Tetraodon nigroviridis* CAG05807 (145/252, 57%); zebrafish *Danio rerio* NP_775349 (178/311, 57%); beetle *Tribolium castaneum* XP_969232 (180/305, 59%); fruitfly *Drosophila melanogaster* NP_648182 (186/311, 59%); fungus *Cryptococcus neoformans* XP_572003 (176/316, 55%); rice *Oryza sativa* EAY89464 (192/304, 63%); mustard *Arabidopsis thaliana* NP_180443 (192/305, 62%); bacterium *R. rubrum* YP_428334 (311/311, 100%). Tgds sequences: human *H. sapiens* NP_055120; mouse *M. musculus* EDL00567; chicken *G. gallus* XP_416988; frog *Xenopus laevis* NP_001088301; zebrafish *Danio rerio* NP_956111; mustard *A. thaliana* NP_564633; rice *O. sativa* NP_001049724; bacterium *R. rubrum* YP_425086. Clustal-X alignment is available on request; sequences were trimmed to include only unambiguously aligned sequences.

Comparison of human and R. rubrum proteomes

We downloaded the human proteome from Ensembl (Birney et al., 2004; Kasprzyk et al., 2004) using NCBI v36 of the human genome obtained from Ensembl version 41. From the US Department of Energy Joint Genome Institute (http://www.jgi.doe.gov/), we obtained the genome sequence of the bacterium *R. rubrum*, strain ATCC 11170. To rank the conservation of Uxs1 relative to other proteins, we performed a BLASTp search using each human protein as a query against a database of all *R. rubrum* proteins using WU-BLAST (http://blast.wustl.edu/) with the BLOSUM62 substitution matrix (Henikoff and Henikoff, 1992) and recorded only BLAST hits with an E-value less than 1×10^{-5}. We used a gap opening penalty of 11 and a gap extension penalty of 1.

Purification of wild-type human UDP-xylose synthase

Human *UXS1* cDNA was purchased from ATCC® (catalog number 10658721). For protein expression, a construct lacking the 84 residue N-terminal transmembrane domain was cloned into a Pet-15b expression vector (Invitrogen) that was modified to include a tobacco etch virus protease cleavage site in place of the thrombin site following the N-terminal 6-His tag. The 84-residue truncation was necessary to express soluble protein, and was based on the deposited crystal structure of human UXS1 in complex with UDP (PDB entry 2B69). UXS1 expression was induced from 4 l of logarithmically growing cells (OD600 ~1.0) after reducing temperature to 20° and adding IPTG (Sigma-Aldrich) to a final concentration of 0.1 mM. Cells were harvested after 6 h and lysed by sonication. The His-tagged UXS1 was purified with Talon(R) affinity resin (Clontech) and eluted with 250 mM imidazole (Sigma-Aldrich). The His tag was removed with a codon-optimized tobacco etch virus protease (van den Berg et al., 2006). The cleaved protein was dialyzed into 20 mM Tris pH 8.0, 250 mM NaCl and concentrated to 11 mg/ml.

Generation of human UDP-xylose synthase R236H

A human wild-type *UXS1* clone (above) was mutagenized with QuikChange™ site-directed mutagenesis kit (Agilent Technologies-Stratagene). DNA sequencing confirmed the human *UXS1* clone mutation, resulting in an enzyme incorporating histidine instead of arginine at amino acid position 236, equivalent to zebrafish *mow*^{w36} mutation, Uxs1 R233H. Purification proceeded as for wild-type UXS1 (above).

Determining UDP-xylose synthase activity

Human wild-type UXS1 or human UXS1 R236H (10 µg) was incubated (18 h, 37 °C) with substrate UDP-glucuronic acid (1 mM) in reaction buffer (100 mM sodium phosphate pH 6, 10 mM dithiothreitol, 1 mM EDTA). Protein was precipitated with acetonitrile and soluble compounds were resolved by capillary zone electrophoresis for 25 min at 22 V (3D-CE ChemStation, Agilent) in 50 mM sodium borate pH 9.0. Peaks were identified with known standards.

Reverse transcriptase-PCR

Total RNA was extracted using Tri Reagent kit (Molecular Research Center Inc., Catalog # TR-118) according to manufacturer's instructions. Superscript III RNase H-reverse transcriptase (Invitrogen, #18080-044) and oligo(dT) primers synthesized first strand cDNA. Reverse transcriptase was heat inactivated and RNA was degraded with RNaseH (Biolabs, M0297S). Primers for *uxs1* were Uxs1.1251+ and Uxs1.1685− and for *actin* were as described (Krovel and Olsen, 2004).

Fluorescent cell labeling

Crosses produced homozygous *mow*^{w60} and *uxs1*^{hi3357} mutants carrying *Tg(fli1:EGFP)y1* (Lawson and Weinstein, 2002), which we imaged live by confocal microscopy. Larvae were grown in 15 mg/L PTU to minimize pigment. One day prior to observation, 200 µl of 0.3% Alizarin red was added to the water to visualize bone. Z-sections at 1.5 µm intervals were taken ventral to dorsal at 20x and 0.25 µ at 60x on a Zeiss confocal microscope.

Whole-mount in situ hybridization

Expression analysis was performed as in Jowett and Yan (1996). A 625 bp antisense probe in the 5' untranslated region (UTR) of *uxs1* was amplified from a 2 dpf (days post fertilization) cDNA library using primers Uxs1.1252 and Uxs1.1877. Probes for *sox9b*, *sox9a*, *ptc1*, *ptc2*, *runx2b*, *col2a1a*, *col10a1*, *runx2a*, *ihha*, *ihhb*, *gli3*, and *erm* were as described (Avaron et al., 2006; Yan et al., 1995; Yan et al., 2002; Yan et al., 2005).

Detection of ECM components

Alcian blue (cartilage) and Alizarin red (bone) double staining was performed as described (Walker and Kimmel, 2007). Wheat germ agglutinin (WGA) staining was performed using biotinylated succinylated WGA (Vector Laboratories, Catalog #B-1025 S) as described (Lang et al., 2006). Whole-mount antibody staining for heparan sulfate (α-HS) (USBiological, Catalog# H1890), chondroitin sulfate (α-CS) (Sigma, product #C8035), and type II collagen (α-Col2a1) (Polysciences, Inc., Catalog# 23707) was conducted by fixation in 4% paraformaldehyde, dehydration with 100% methanol, rehydration with PBST followed by digestion with 0.1% trypsin at 37 °C for 2 h and 30 min for 5 and 3 dpf, respectively. Following two PBST rinses, α-HS and α-Col2a1 samples were incubated with 0.5% hyaluronidase (USBiological, Catalog # D-H7981-01) in 1× PBST for 30 min at 37 °C, followed by PBDT washes. Blocking solution was added to tubes containing 2% goat serum in PBDT for 2 h. Antibodies α-HS, α-CS, and α-Col2a1 were added at 1:200, 1:100, and 1:100 dilution respectively and incubated overnight at 4 °C. Secondary antibodies goat-α-rabbit-HRP for α-Col2a1, goat α-mouse-Alexa488 for α-CS and goat-α-mouse-AP for α-HS were used at 1:1000. Histochemical detection of antibody was carried out with VECTASTAIN ABC Reagent kit (Vector Laboratories, Cat. No. PK-4000) and NBT/BCIP, respectively.

Results

Chondrogenesis and osteogenesis require mow function

A screen of mutagenized chromosomes identified *man-o'-war* (*mow*^{w60}), a mutant phenotype that, like *jellyfish* (*sox9a*) (Piotrowski et al., 1996; Yan et al., 2002), lacks Alcian blue-positive, neural crest-derived cartilages. Compared to wild-type siblings at 5 days post fertilization (5 dpf), homozygous *mow*^{w60} mutants lacked tissue anterior to the eyes and had reduced lower jaw, a shortened body axis, and small pectoral fins (Fig. 1A, B, E and F; and data not shown). Histological staining of skeletal tissues showed that 7 dpf homozygous *mow*^{w60} embryos lacked robust Alcian blue-positive pharyngeal and neurocranial cartilages (Fig. 1C, D, G and H), including Meckel's cartilage, ceratohyal, palatoquadrate, and ceratobranchials. Alizarin red, which marks ossification centers, identified reduced bone formation in *mow*^{w60} embryos. For example, the parasphenoid, 5th ceratobranchial, and opercle showed Alizarin red staining in *mow*^{w60} embryos, but these skeletal elements were much smaller than those in wild types. Compared to wild types, homozygous *mow*^{w60} mutants also had fewer Alizarin red-positive skeletal elements, such as the

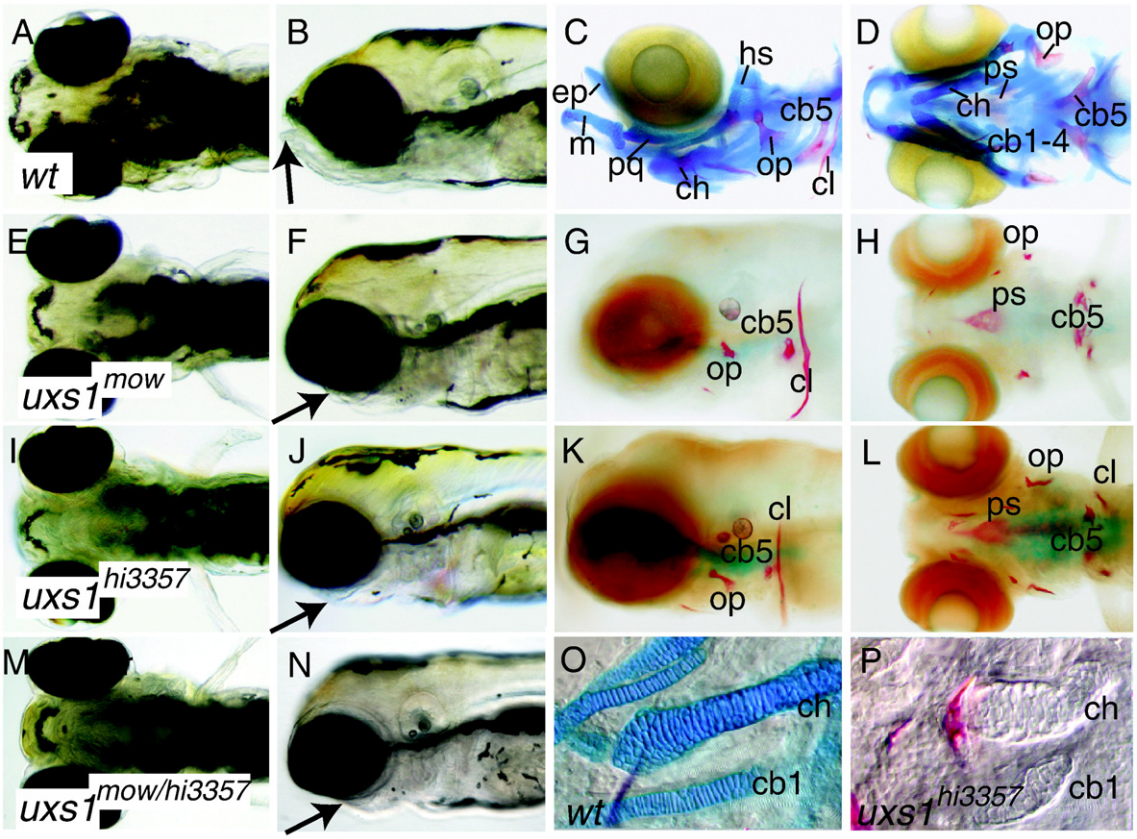

Fig. 1. Craniofacial and skeletal phenotypes of zebrafish larvae. Ventral and lateral views of live (A, B, E, F, I, J, M, N) and Alcian blue-, Alizarin red-stained (C, D, G, H, K, L, O, P) animals. Compared to wild types (A, B), mutant animals (E,F *mow*^{w60} allele; I, J *hi3357* allele) had reduced lower jaws (arrows) at 5 dpf. Reduced lower jaw (arrow) in *mow*^{w60}/*hi3357* double heterozygotes (M, N) showed failure of complementation. Alcian blue and Alizarin red staining for cartilage (blue) and bone (red) revealed the lack of cartilage and reduced bones in mutants (G, H, K, L) compared to wild type (C, D) at 7 dpf. Nomarski optics on dissected pharyngeal skeletons suggested that mutant cartilages (P) condensed in the same areas as wild types (O), but did not secrete Alcian blue-positive matrix. Abbreviations: cb1-5, ceratobranchials 1 to 5; ch, ceratohyal; cl, cleithrum; ep, ethmoid plate; hs, hyosymplectic; m, Meckel's cartilage; op, opercle; pq, palatoquadrate; ps, parasphenoid.

ceratohyal and hyosymplectic. Because the parasphenoid, opercle, and cleithrum develop by intramembranous ossification, and the hyosymplectic, ceratohyal, and 5th ceratobranchial develop by endochondral ossification (Cubbage and Mabee, 1996; Renn et al., 2006), both mechanisms of bone formation appear to depend upon wild-type *mow*^{w60} function.

Our mapping data (see Fig. 2) suggested that *mow*^{w60} and the *hi3357* retroviral insertion mutation (Amsterdam et al., 2004; Golling et al., 2002; Nissen et al., 2006) could be alleles, so we performed similar gross morphological and histological analyses of *hi3357*. Indeed, we found that *hi3357* shared the same morphological and histological defects as observed in *mow*^{w60} (Fig. 1I–L). Crossing a heterozygous *mow*^{w60} male to a heterozygous *hi3357* female gave 21 of 98 (21.4%) animals with the mutant phenotype (Fig. 1M and N), as expected if *mow*^{w60} and *hi3357* fail to complement and thus disrupt the same gene. Dissections and flat-mounts of pharyngeal cartilages suggested that chondrogenic cells had reached their appropriate anatomical locations and condensed normally in *hi3357* mutants (Fig. 1O and P). These results show that the *mow*^{w60} and *hi3357* mutations interrupt a gene essential for deposition of the Alcian blue-positive extracellular matrix of cartilage and normal bone morphogenesis in zebrafish.

mow^{w60} *and hi3357 disrupt uxs1*

To identify the molecular genetic defect responsible for the *mow*^{w60} phenotype, we generated an F_2 mapping population. A genome scan using simple sequence repeats (SSRs) (Knapik et al., 1998; Shimoda et al., 1999) and bulk segregant analysis, showed that z3124, z9112 and z6663 on linkage group nine (LG9) were linked to the mutant locus. The genotyping of 480 individuals from the F_2 mapping panel mapped *mow* about 20 cM from z3124 (Fig. 2A). A search of ZFIN (http://zfin.org) for mutants near *mow* identified the pro-viral insertion *hi3357*, the preliminary characterization of which showed decreased Alcian blue staining (Amsterdam et al., 2004; Golling et al., 2002; Nissen et al., 2006) (see our Fig. 1I–L). To see if *mow* maps near *hi3357*, we used BLAST to search the zebrafish genome for sequence flanking *hi3357* and identified on Zv4_scaffold346 an SSR from intron-7 of *uxs1*, the predicted gene near the insertion. We genotyped our *mow* mapping panel using mapping primers flanking this SSR, and learned that this SSR mapped less than 0.5 cM from *mow*, as expected if *mow*^{w60} and *hi3357* disrupt the same gene.

Sequences flanking the *hi3357* insert are similar to the human *UDP xylose synthase 1* (*UXS1*) gene (Amsterdam et al., 2004; Golling et al., 2002). Evidence that this sequence is the zebrafish ortholog of *UXS1* comes from phylogenetic analysis and conserved syntenies. A neighbor-joining phylogenetic tree of amino acid sequences from organisms as diverse as humans and prokaryotes (Fig. 2B) shows that the protein disrupted by *mow*^{w60} and *hi3357* falls in the Uxs1 clade of the tree, well-separated from the next most similar clade, Tgds (TDP-glucose 4,6-dehydratase), which itself has a zebrafish ortholog (NP_956111). Analysis of conserved syntenies confirms orthologies: the sequence lying to the immediate right of *uxs1* on zebrafish LG9 is zgc:112443, whose reciprocal best BLAST hit in the human genome is *ECRG4*, which lies adjacent to *UXS1* on human chromosome 2. The

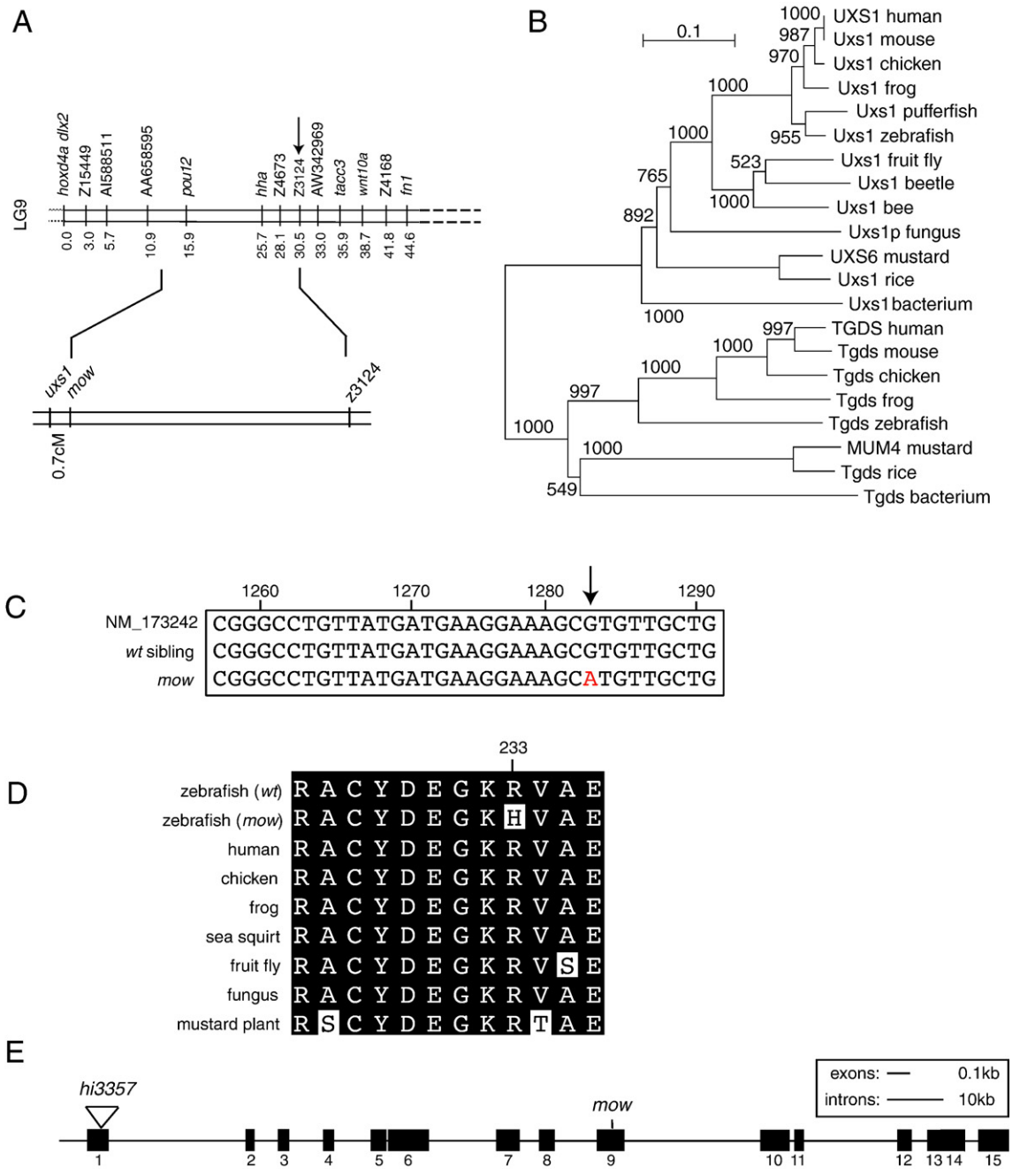

Fig. 2. Mapping, cloning, and sequencing of *mow*. (A) LG9 from the HS panel above (Woods et al., 2005) and the interval mapped on the *mow* mapping panel below. Distances are in centiMorgans (cM). (B) Phylogenetic tree of proteins retrieved by BLASTP search of NCBI, aligned by Clustal-X, and analyzed by neighbor joining showed that the zebrafish protein disrupted by mow^{w60} falls in the Uxs1 clade, well-separated from the next most closely related protein, TGDS. Sequences and sequence identities listed in Materials and methods. (C) Nucleotide sequence comparison of *uxs1* from homozygous mow^{w60} mutants to wild-type siblings and reference sequence NM_173242 revealed a G-to-A replacement at nucleotide position 1283 (arrow). (D) Amino acid sequence alignment of the portion of Uxs1 corresponding to the nucleotides shown in part C for zebrafish (WT), zebrafish (mow^{w60}) with the arginine (R) to histidine (H) substitution at position 233, human, chicken, frog *Xenopus tropicalis*, sea squirt *Ciona intestinalis* (translated from genomic sequence, CINT1.95:scaffold_505), fruit fly *Drosophila melanogaster* (CG7979-PA), fungus *Cryptococcus neoformans* (AAM22494) and mustard plant *Arabidopsis thaliana* (NP_190920). Unless otherwise noted, sequences were the same as those used in panel B. (E) Structure of the zebrafish *uxs1* gene, showing the location of the *hi3357* viral insert in exon 1 (Amsterdam et al., 2004; Golling et al., 2002; Nissen et al., 2006) and the position of the mow^{w60} nucleotide substitution in exon 9.

proximity of these neighbors (*UXS1* and *ECRG4*) has been conserved for 450 million years since the divergence of human and zebrafish lineages (Hedges, 2002).

To identify the induced molecular change in mow^{w60}, we sequenced overlapping fragments amplified across *uxs1* from mutant cDNA template and found eight nucleotide differences from the reference sequence NM_173242: four differences are present in ESTs of wild-type zebrafish and thus represent naturally occurring polymorphisms; one causes a synonymous change; two are in the 5' untranslated region; and one changes a guanine (G) to adenosine (A) at nucleotide position 1283 in the highly conserved exon 9 (Fig. 2C and E). The G1283A change replaces arginine 233 with histidine (R233H) in a ten amino acid portion of the Uxs1 protein that is nearly invariant among all sequenced animals and fungi (Fig. 2D). In

summary, our genetic mapping data and gene sequencing data support the inference from the complementation study (Fig. 1M and N) that *mow*^{w60} and *hi3357* disrupt the same gene, *uxs1*.

Uxs1 is one of the most strongly conserved non-mitochondrial proteins

Sequence alignments showed remarkably strong conservation of Uxs1 sequence across all three domains of life. Compared to the Uxs1 of the prokaryote bacterium *R. rubrum*, eukaryotes have 55% to 63% identity (vertebrates, such as human, mouse, chicken, frog, and fish, had 57% amino acid identity; insects, such as fruit fly and beetle, 59%, a fungus (*C. neoformans*) 55%; and plants, such as rice and mustard, 62–63%). An archaebacterium, for example *Methanocaldococcus vulcanius*, has 51%, while other bacteria have about 50% or more identity (*Rhizobium leguminosarum*, 54%, *Escherichia coli, 68%, Thermotoga neapolitana*, 49%). To see how Uxs1 ranks on a list of conserved proteins, we compared the human proteome to the proteome of the bacterium *R. rubrum* by BLAST analysis, ranked the results by E-value, and examined the literature for sub-cellular localization of each hit, ruling out mitochondrial proteins encoded by nuclear or mitochondrial genomes. Results showed that Uxs1 (E-value = 2.10E−100) ranked fifth on the list after GPI, IDH1, ADH5, and GMDS, which had E-value scores of 2.80E−179 to 2.20E−117 and % identities of 61% to 66%. We conclude that the amino acid sequence of Uxs1 has been one of the most strongly conserved proteins for over 3 billion years of biological evolution.

Molecular function and structure of mutant Uxs1

Because it disrupts sequences directly upstream of translation initiation, *uxs1*^{hi3357} is likely a null allele (Fig. 2E). Given the phenotypic similarity of *mow*^{w60} to *uxs1*^{hi3357}, we wanted to determine whether *mow*^{w60} is also a null allele and to try to understand why Uxs1 is so strongly constrained for life on Earth. Zebrafish Uxs1 shares 86% sequence identity to the human enzyme, with most sequence diversity residing in the amino terminal transmembrane domain. The soluble domains of Uxs1 that include arginine 233 share 96% sequence identity between zebrafish and human. To determine whether the arginine-to-histidine replacement observed in *mow*^{w60} changes a site essential for enzyme activity, we replaced the equivalent arginine with a histidine in the human enzyme (R236H; hereafter all residues are referred to with zebrafish numbering, i.e. R233H). We then assayed the wild-type and mutant enzymes for activity. Results showed that the mutant enzyme did not convert the substrate UDP-glucuronic acid to the product, UDP-xylose, but the wild-type enzyme made this conversion readily (Fig. 3A). This result shows that the substitution of arginine by histidine at this position is sufficient to eliminate the enzymatic function of Uxs1 protein.

Using the unpublished, publicly available crystal structure of human UXS1 (The Structural Genomics Consortium, PDB entry 2B69), we modeled the zebrafish R233H mutation. The crystal structure of UXS1 revealed a homodimer with each subunit containing a molecule of nicotinamide adenine dinucleotide (NAD) bound in the active site (Fig. 3B). Arg233 is buried in the dimer interface about 16 Å distant from NAD, and it appears to stabilize the dimer interface. The guanidinium of Arg233 makes hydrogen bonds with the main-chain carbonyl oxygen atoms of Trp216 and Val202 (Fig. 3C). Arg233 also interacts with residues from the other subunit by making a salt-bridge with Glu230 and a hydrogen bond to the main-chain carbonyl oxygen of Val219.

Our modeling predicts that mutating Arg233 to histidine would disrupt the dimer interface because a histidine cannot satisfy the salt-bridge with Glu230 without introducing unfavorable contacts throughout the interface. Dimerization of the R233H mutant would bury the two acidic residues (one from each subunit) without a basic residue to neutralize the charge. Burying an uncompensated acid is energetically costly and will destabilize protein structure (Dao-pin et al., 1991). In addition, histidine cannot satisfy the extensive hydrogen bonding network supported by the guanidinium of Arg233 (Fig. 3D). The carbonyl oxygens of Trp216 and Val219 of the other subunit are 3.3 Å apart, which would result in unfavorable electrostatic interactions in the absence of Arg233. Finally, histidine is not isosteric to the well-packed Arg233, and its bulky imidazole ring in place of the alkyl portion of the arginine side chain would introduce unfavorable contacts in the interface. Crystallographic analysis of an arginine-to-alanine substitution at this position in human UXS1 indicates local secondary structure disordering at the dimer interface (SJP and ZAW, *in prep.*). This evidence shows that the zebrafish R233H mutation should disrupt the Uxs1 dimer, thereby abolishing enzyme activity.

Expression of uxs1 in zebrafish development

If the phenotype of *mow*^{w60} is caused by disruption of *uxs1*, then *uxs1* should be expressed in craniofacial regions at or before the developmental defect becomes apparent. RT-PCR and whole-mount *in situ* hybridization experiments showed that one-cell embryos have maternal *uxs1* transcript (Fig. 4A and B). Under the RT-PCR conditions used, *uxs1* signal decreased during epiboly and increased during segmentation stages (Fig. 4A), as if maternal mRNA gradually disappeared and was replaced by zygotic transcript. At 24 hpf, *in situ* hybridization on sectioned and whole-mounted embryos revealed *uxs1* transcript in ventral craniofacial domains and along the yolk-endoderm boundary (Fig. 4C and D). At 2 and 3 dpf, *uxs1* transcripts were broadly distributed throughout the head, appearing in the pharyngeal arches, eye, fin bud, neurocranium, notochord, and brain (Fig. 4E and F). At 5 dpf, *uxs1* expression localized to the developing pharyngeal arch cartilages in both chondrocytes and perichondrium (Fig. 4G and G′). We also observed that *uxs1* transcript is diminished in *uxs1*^{hi3357} larvae at 5dpf (Fig. 4H and H′), suggesting that transcript containing the viral insert is unstable. These results show that *uxs1* transcript is localized in a pattern consistent with the mutant craniofacial phenotype, and that transcript instability may contribute to the loss of *uxs1* function in *uxs1*^{hi3357} larvae.

uxs1 mutants show altered morphogenesis of cartilage, perichondrium, and dermal bone

To identify cellular mechanisms responsible for the disruption of skeletal development in *uxs1* mutants, we crossed *uxs1* mutant alleles into the transgenic line *Tg(fli1:EGFP)y1*, which expresses green fluorescent protein (GFP) in developing skeletogenic neural crest cells (Lawson and Weinstein, 2002). Dual-channel confocal microscopy of vital Alizarin red-stained wild-type and mutant larvae of the *Tg(fli1:EGFP)y1*;*uxs1*^{hi3357} and *Tg(fli1:EGFP)y1; mow*^{w60} strains highlighted both crest-derived chondrocytes and bone calcification centers in living animals. In 4 dpf wild types, cells had already begun to stack in craniofacial cartilages (Fig. 5A and E). In 4 dpf *uxs1* mutants, however, chondrocytes did not intercalate with their neighbors and stack normally (Fig. 5C and G). In 7 dpf wild-type larvae, chondrocytes maintained their intercalated and stacked organization, and the bone collar had started to form around the central portion of the ceratohyal (Fig. 5B and F). Additionally, Alizarin red staining revealed the growth of dermal bones, such as the dentary, which by 7 dpf had proceeded laterally from its location in 4 dpf larvae. In 7 dpf *uxs1* mutants, however, chondrocytes remained rounded, with little intercalation, and were spatially disorganized (Fig. 5D and H). Likewise, the mutant dentary showed defective morphogenesis, failing to extend as far laterally as in wild-type animals (compare Fig. 5B–D). The perichondrium, which depends on signaling from chondrocytes, was not well organized in mutants, lacking the continuous flattened layer of cells seen in wild types (compare Fig. 5F–H, arrows). At both 4 and 7 dpf,

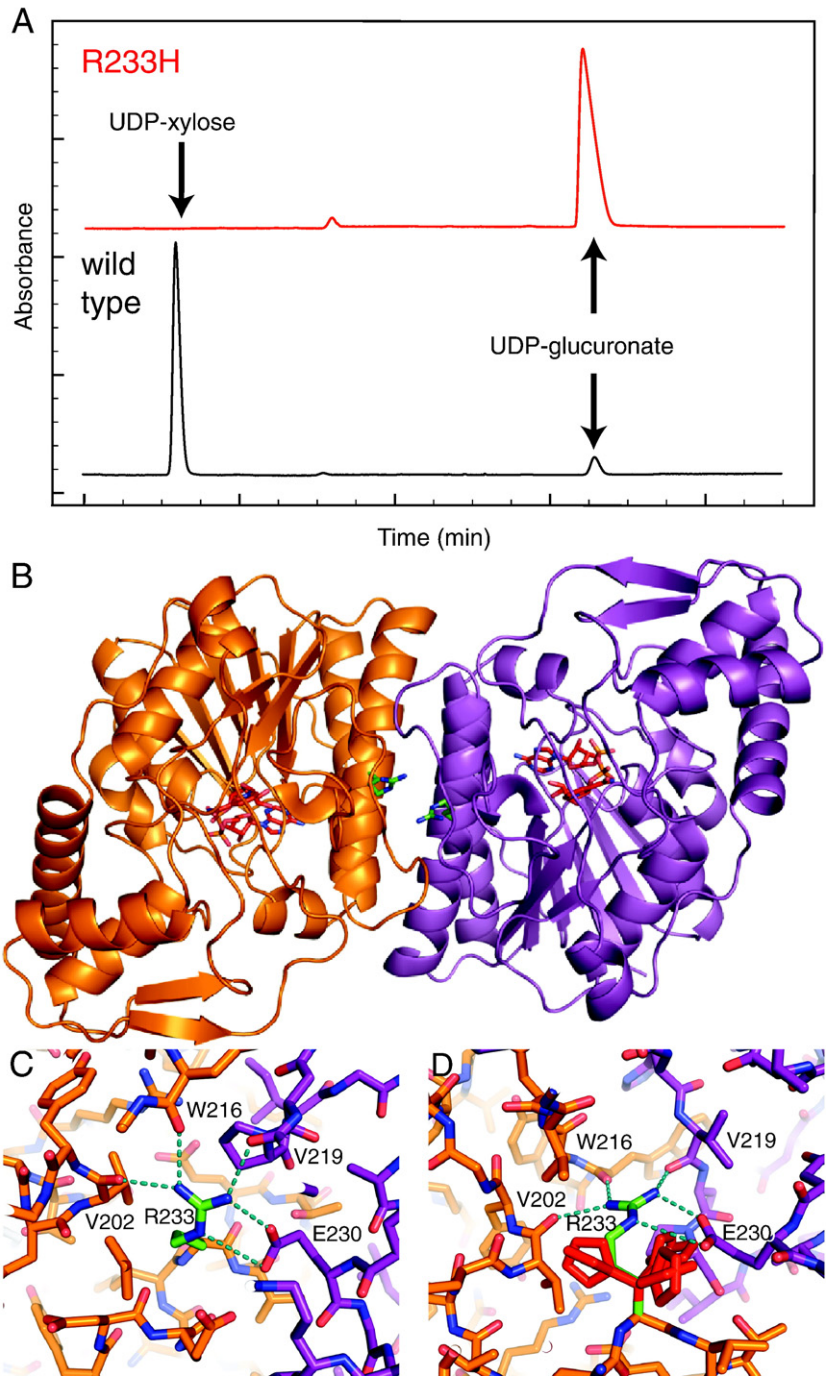

Fig. 3. Effects of the *mow*^{w60} mutation on Uxs1 function and structure. (A) Capillary zone electrophoresis chromatogram of enzyme reactions catalyzed by wild-type human UXS1 (lower black trace) or mutated UXS1 corresponding to the zebrafish *mow*^{w60} (R233H, upper red trace). Peaks represent absorbance at 260 nm and are on the same scale, but offset vertically for ease of comparison using Plot (http://plot.micw.eu). UXS1 with the *mow*^{w60} mutation produced no detectable enzyme product, UDP-xylose, after an 18 h incubation with substrate (UDP-glucuronate) at 37 °C but the wild-type enzyme converted nearly all of the substrate into product. (B) Ribbon drawing of the crystal structure of dimerized human UXS1 (PDB entry 2B69), with different monomers colored orange and purple. NAD (red and blue) and the side chains corresponding to zebrafish R233 (green and blue) are depicted as sticks. (C, D) Conserved hydrogen bonding and salt bridge interactions (dashed pale blue lines) revealed the structural consequences of the zebrafish R233H substitution (D) at the dimer interface, compared to wild-type (C). The histidine (red sticks in D) was modeled in several of its common rotomeric states to illustrate the unfavorable contacts it introduces and its inability to satisfy the electrostatic interactions of the R233 guanidinium. Depiction of R233 (green sticks) provided as a frame of reference. Numbering corresponds to zebrafish residues. Figure generated using Pymol (DeLano, 2002).

the ceratohyal showed no clear difference in cell number between mutants and wild types, although mutant cartilage elements appeared shorter, suggesting a failure in elongation. These data demonstrate that *uxs1* functions in many aspects of skeletal morphogenesis, helping chondrocytes intercalate and stack, driving cartilage elongation, and directing perichondral and dermal bone morphology.

Proteoglycan levels are reduced in uxs1 mutants

We next sought to identify molecular alterations in the mutant ECM that might provide a mechanism for observed defects in skeletal histogenesis and morphogenesis. To investigate whether *uxs1* is required for normal proteoglycan biosynthesis, we used biotinylated-succinylated

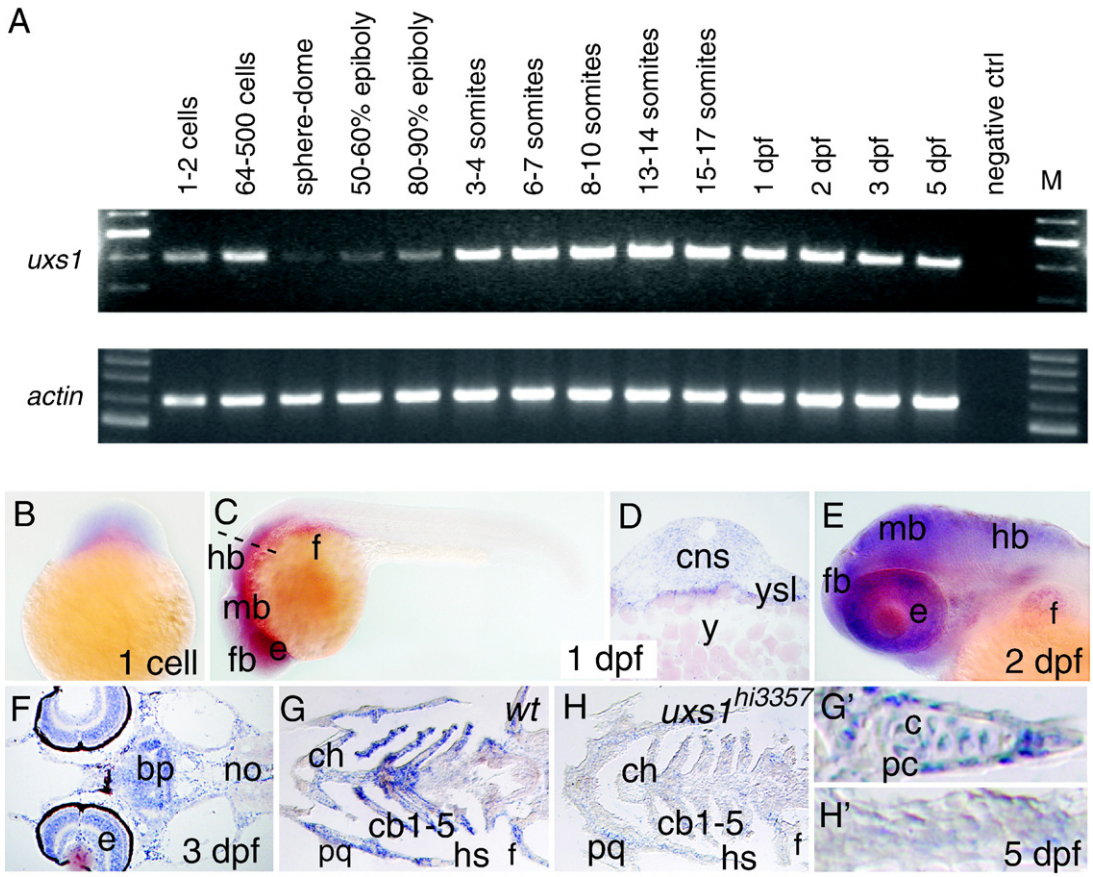

Fig. 4. *uxs1* expression during zebrafish embryogenesis. (A) RT-PCR for *uxs1* transcript in animals of indicated ages, along with *β-actin* positive controls. Maternal *uxs1* mRNA was detected at the 1–2 cell stage and detection decreased at sphere-dome stage. Zygotic *uxs1* expression appeared to increase gradually and was maintained at least through 5 dpf. (B) Whole-mount *in situ* hybridization of a one-cell embryo revealed transcript in the fertilized egg. (C, D) Whole-mount (C) and section (D) of 24 hpf embryos illustrated general expression of *uxs1* in brain and craniofacial mesenchyme, as well as in the yolk syncytial layer. The dashed line in panel C indicates the plane of section in panel D. (E) Lateral view of whole-mount 2 dpf embryo showed widespread *uxs1* expression in the craniofacial region. (F–H) Horizontal sections of 3 dpf (F) and 5 dpf (G,H) animals. Expression of *uxs1* became localized to layers of the retina, brain, and cartilages of the pharyngeal arches. Levels of *uxs1* transcript were severely reduced or absent in pharyngeal regions of *uxs1*^{hi3357} embryos. High magnification of 5 dpf ceratohyals shows *uxs1* expression in both chondrocytes (c) and perichondral cells (pc) of wild types (G'), but low transcript levels in *uxs1*^{hi3357} embryos (H'). Abbreviations: bp, basal plate; c, chondrocyte; cb1-5, ceratobranchials 1-5; ch, ceratohyal; e, eye; f, fin bud; fb, forebrain; hb, hindbrain; hs, hyosymplectic; mb, midbrain; no, notochord; pc, perichondrium; pq, palatoquadrate; y, yolk; ysl, yolk syncytial layer.

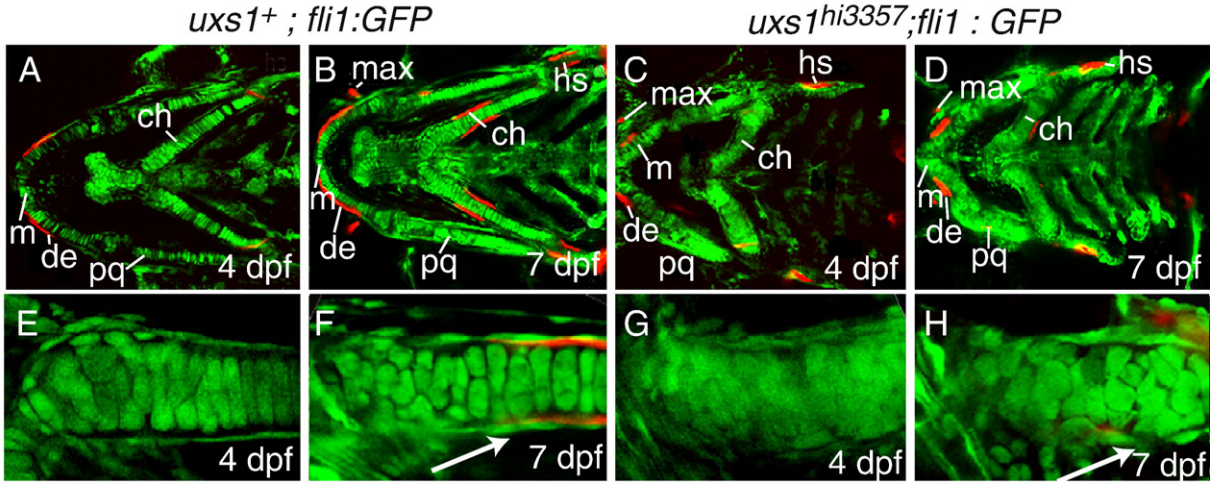

Fig. 5. Cellular visualization of cartilage and bone morphologies in wild-type and *uxs1* mutant larvae. (A–H) Optical sections of live Alizarin red-stained *Tg(fli1:EGFP)y1* larvae, ventral views, at 4 dpf and the same individuals at 7 dpf. (E–H) Focus on the ceratohyal. In wild types (A, B, E, F), chondrocytes stacked and were lined with a flattened layer of perichondral cells (white arrow in F). Ossification centers stained with Alizarin red, reflecting perichondral bone formation in the ceratohyal and hyosymplectic and intramembranous ossification in the dentary and maxilla. In homozygous *uxs1*^{hi3357} animals (C, D, G, H); however, chondrocytes were disorganized, the perichondral sheath did not align properly (white arrow in H), and Alizarin red-positive ossification centers (dentary, maxilla, and ceratohyal) were severely reduced in perichondral and intramembranous sites. Abbreviations: ch, ceratohyal; de, dentary; hs, hyosymplectic; m, Meckel's cartilage; max, maxilla; pq, palatoquadrate.

wheat germ agglutinin (WGA) to stain *N*-acetylglucosamine, a sugar found in the GAG chains of cartilage proteoglycans (Lang et al., 2006). In wild types at 5 dpf, WGA localized to cartilages of the pharyngeal arches (Fig. 6A). At higher magnification, WGA staining appeared in organized layers between cells in the palatoquadrate and in ceratobranchial-1 (Fig. 6C). WGA-positive material also appeared in intracellular foci (data not shown), possibly due to *N*-acetylglucosamine within the Golgi complex of chondrocytes. In homozygous *uxs1*^{hi3357} and *mow*^{w60} mutants; however, WGA was reduced or absent in cartilages of the pharyngeal arches, including the ceratohyal and Meckel's cartilage (Fig. 6B, and data not shown). Moreover, cartilage morphologies were disorganized, and WGA staining was irregularly dispersed between limited numbers of cells in mutants (Fig. 6D). In the appendicular skeleton of wild types, the endoskeletal disc stained with WGA and abundant actinotrichia formed a filamentous fin tip (Fig. 6E). Homozygous *uxs1* mutants, however, showed little WGA staining in their diminutive endoskeletal discs and their actinotrichia were reduced in number and stained poorly (Fig. 6F).

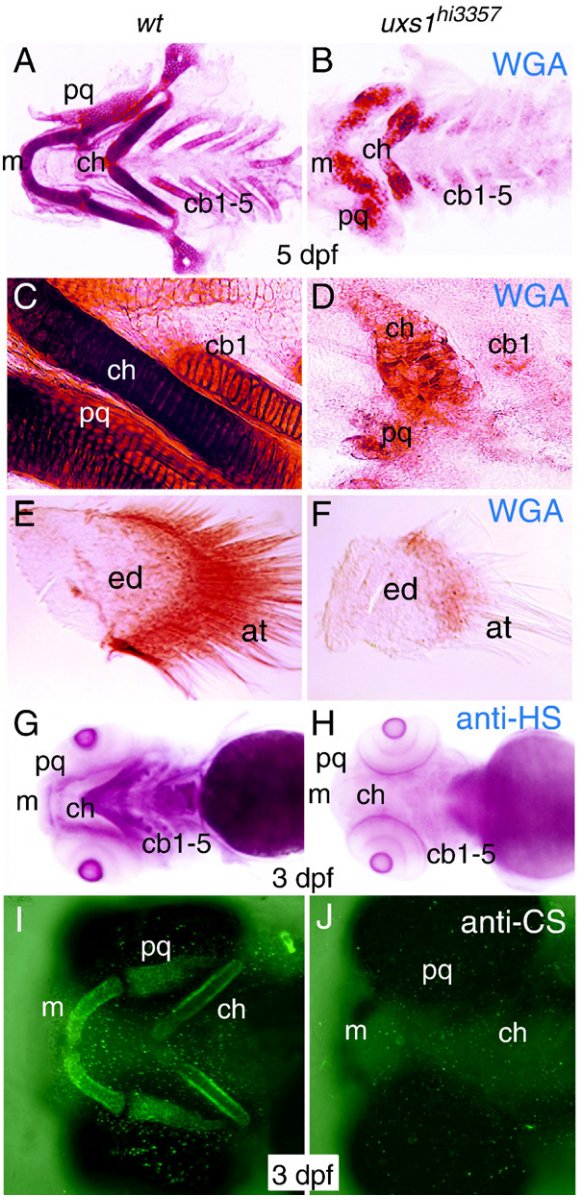

Fig. 6. Proteoglycan detection in wild-type and *uxs1* mutant skeletons. (A–F) Whole-mount wheat germ agglutinin (WGA) staining to visualize *N*-acetylglucosamine, ventral views. (G–J) Whole-mount immunostaining against heparan sulfate (G, H) and chondroitin sulfate (I, J) proteoglycans, ventral views. Dissected pharyngeal cartilages revealed reduced WGA staining in *uxs1*^{hi3357} mutants (B, D), compared to wild-type siblings (A, C) at 5 dpf. Higher magnification of ceratohyal regions also showed that WGA-positive material was not deposited normally in mutants (D), compared to organized deposition in wild types (C). Dissected pectoral fins showed that both endoskeletal disc and actinotrichia had less WGA staining and fewer actinotrichia in *uxs1*^{hi3357} mutants (F), compared to wild-type siblings (E) at 5 dpf. Immunodetection of heparan sulfate demonstrated that HSPGs were localized to pharyngeal domains in wild type (G), but HSPGs were not detectable in homozygous *uxs1*^{hi3357} animals (H). Similarly, immunodetection of chondroitin sulfate was abundant in wild-type cartilages (I), but was absent in *uxs1* mutants (J). Abbreviations: at, actinotrichia; cb1-5, ceratobranchials 1-5; ch, ceratohyal; ed, endoskeletal disc; m, Meckel's cartilage; pq, palatoquadrate.

If *uxs1* mutants fail to make UDP-xylose for the tetrasaccharide linker, then they should not produce heparan sulfate or chondroitin sulfate proteoglycans (HSPGs, CSPGs). In wild types at 3 dpf, heparan sulfate antibody (α-HS) identified HSPGs in pharyngeal arches and pectoral fin (Fig. 6G). In homozygous *uxs1* mutant heads, however, staining disappeared (Fig. 6H), showing that *uxs1* activity is essential for the formation of HSPGs. Similarly, immunodetection of CSPGs was abundant in wild-type cartilage at 3 dpf, but *uxs1* mutants failed to show any evidence of CSPGs (Fig. 6I and J). Together, these results show that *uxs1* function is required for proteoglycan expression and localization in pharyngeal cartilages, and is necessary for normal development of pectoral appendages.

Uxs1 activity regulates expression of skeletal collagens

Surprisingly, we discovered that proper expression of collagenous ECM components relied on Uxs1-dependent proteoglycan production. First, we investigated the expression of *col2a1a*, which encodes a major collagen of cartilage (Hamerman, 1989; Yan et al., 1995). Compared to wild-type siblings, homozygous *uxs1* mutant embryos at 3 dpf had increased levels of *col2a1a* transcript in craniofacial cartilage elements (Fig. 7A and B). *In situ* hybridization of sections of 5 dpf larvae confirmed increased *col2a1a* transcript levels in developing chondrocytes of *uxs1* mutant ceratohyals (Fig. 7C and D). Differences between wild types and *uxs1* mutants were also apparent upon analysis of Col2a1 protein. Immunohistochemistry revealed that Col2a1 was present in all craniofacial cartilages and in the fin in wild types at 5 dpf (Fig. 7E). In contrast, Col2a1 protein was almost completely absent from craniofacial cartilages of homozygous *mow*^{w60} and *uxs1*^{hi3357} mutants and was greatly reduced in the fin (Fig. 7F, and data not shown). These results show that *uxs1* normally inhibits the accumulation of *col2a1a* transcripts, but, somewhat paradoxically, promotes the deposition and/or maintenance of stainable Col2a1 protein in the extracellular matrix.

Type X collagen (Col10a1) is a marker of both osteoblasts and maturing chondrocytes in teleosts (Avaron et al., 2006; Clement et al., 2008; Simoes et al., 2006). In wild types, whole-mount *in situ* hybridization at 5 dpf showed that *col10a1* is expressed in osteoblasts of both the endochondral (e.g., ceratohyal, hyomandibular) and intramembranous (e.g., opercle, dentary) skeletons (Fig. 7G and I). In homozygous *uxs1* larvae at 5 dpf, however, *col10a1* expression occurred only in dermal bones, and these expression domains were generally smaller than normal (Fig. 7H and J). Endochondral ossification appeared delayed or absent in *uxs1* mutants at 5 dpf, since perichondral *col10a1* expression is missing from the mutant ceratohyal, but is obvious in wild types at this stage. Because chondrocyte maturation also reflects the degree to which endochondral ossification has progressed, we performed *in situ* hybridization on sections to analyze chondrocyte *col10a1* expression. At 5 dpf, maturing chondrocytes in the mid-diaphyseal region of wild-type ceratohyals expressed *col10a1*, whereas *uxs1* mutants failed to express this marker of chondrocyte maturation (Fig. 7K and L). Collectively, these results demonstrate that *uxs1* function is essential for the induction and/or maintenance of skeletal collagens, such as Col2a1 and *col10a1*, and suggest that the maturation of ceratohyal chondrocytes to the *col10a1*-expressing stage relies upon Uxs1-dependent proteoglycans.

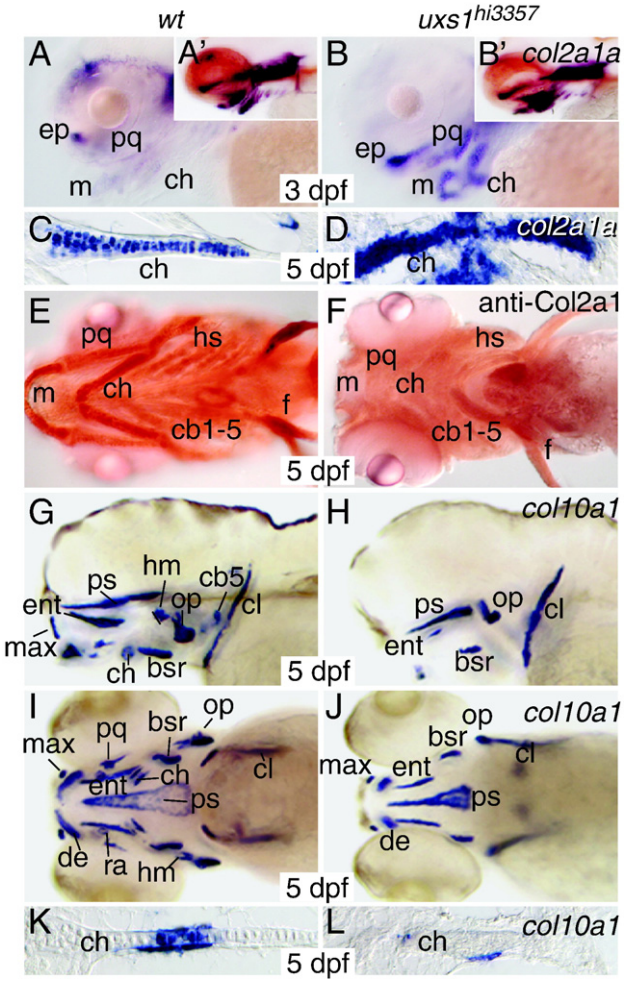

Fig. 7. Collagen detection in wild-type and *uxs1* mutant skeletons. (A–D) Whole-mount (A, B) and horizontal section (C, D) *in situ* hybridization for *col2a1a* gene expression; (E, F) whole-mount immunostaining for Col2 protein; (G–L) whole-mount (G–J) and horizontal section (K, L) *in situ* hybridization for *col10a1* gene expression. Expression of *col2a1a* increased in developing cartilage of *uxs1*^{hi3357} mutants in lateral views of the head at 3 dpf (B) and ceratohyal sections at 5 dpf (D), compared to wild-type siblings (A, C). Longer substrate developing times demonstrated that *col2a1a* levels are high in cartilage of both wild type and mutant heads at 3 dpf (A′, B′). In contrast, although Col2a1 protein was easily detected in wild type cartilages (E) in ventral view at 5 dpf, it was not detected in mutant cartilages (F). Lateral (G, H) and ventral (I, J) whole-mount views showed that domains of *col10a1* gene expression were greatly reduced in regions of endochondral and intramembranous skeletal elements in 5 dpf *uxs1* mutants (H, J), compared to wild types (G, I). *In situ* hybridization on histological sections of the ceratohyal at 5 dpf illustrated reduced perichondral staining of *col10a1* in mutants (L), compared with wild types (K). Also, chondrocyte expression of *col10a1* was absent in mutants, although wild-type ceratohyal chondrocytes strongly expressed *col10a1*. Abbreviations: bsr, branchiostegal ray; cb1-5, ceratobranchials 1-5; ch, ceratohyal; cl, cleithrum; de, dentary; ent, entopterygoid; ep, ethmoid plate; f, fin; hm, hyomandibular; hs, hyosymplectic; m, Meckel's cartilage; max, maxilla; op, opercle; pq, palatoquadrate; ps, parasphenoid.

Uxs1 is upstream of the 'master regulators' of cartilage and bone

The transcription factors Sox9 and Runx2 have been thought of as master regulators of cartilage and bone, respectively (Akiyama, 2008; Eames et al., 2003; Eames and Helms, 2004; Eames et al., 2004; Otto et al., 1997; Yoshida and Komori, 2005). To determine whether the molecular defects in skeletal histogenesis that we discovered in *uxs1* mutants result from Uxs1-dependent expression of these important regulators, we compared the expression patterns of *sox9a, sox9b, runx2a,* and *runx2b* in wild-type and *uxs1* mutant larvae in histological sections.

Ceratohyal cartilages in wild-type zebrafish express *sox9a* in chondrocytes at 3 dpf, but *sox9a* becomes down-regulated at 5 dpf in the mid-diaphyseal region as chondrocytes mature (Fig. 8A and C). In contrast, the ceratohyal of *uxs1* mutants over-expresses *sox9a* and fails to down-regulate *sox9a* on the normal schedule (Fig. 8B and D). We did not detect any differences in *sox9a* expression between wild types and *uxs1* mutants at 48 hpf (data not shown). Therefore, up-regulation of *sox9* in mutants only occurred after chondrogenic cells in wild types began to secrete abundant proteoglycans at 3 dpf, as detected by antibodies to chondroitin sulfate (data not shown). Chondrocytes of the wild-type ceratohyal do not express *sox9b* at 72 hpf, although *sox9b* expression is high in developing chondrocytes at 48 hpf (Fig. 8E, data not shown; (Yan et al., 2005). In *uxs1* mutants, however, weak *sox9b* expression persists inappropriately in ceratohyal chondrocytes at 3 dpf (Fig. 8F). In wild types, *runx2a* and *runx2b* are expressed in the perichondrium of the ceratohyal in 3 dpf larvae (Fig. 8G and I). As would be expected from the previous defects in perichondral bone of *uxs1* mutants, *runx2a* and *runx2b* expression in cells surrounding condensed ceratohyal chondrocytes was decreased (Fig. 8H and J). In addition, *runx2b* expression in chondrocytes of the ceratohyal was up-regulated in *uxs1* mutants compared to wild types at 3 and 5 dpf (Fig. 8I–L). Normal expression of *runx2a* does not occur at high levels in chondrocytes, and we saw no ectopic *runx2a* expression in mutant chondrocytes.

Because FGF signaling drives *sox9* expression in chondrocytes (Coumoul and Deng, 2003; de Crombrugghe et al., 2000; Eames and Schneider, 2008; Itoh and Ornitz, 2004), and because proteoglycans are known to affect FGF signaling (Ornitz, 2000; Pellegrini, 2001), we sought to determine whether the *uxs1* mutation increased *sox9* expression through increased FGF signaling. While transcripts of the FGF-responsive genes *sprouty4* and *pea3* were not detected in chondrocytes of the ceratohyal at 3 dpf (data not shown), *erm* expression was found in few chondrocytes in wild types (Fig. 8M). Supporting the notion that FGF signaling is up-regulated in early cartilages of *uxs1* mutants, *erm* expression was detected at high levels in all mutant chondrocytes (Fig. 8N). From these data, we conclude that *uxs1* normally acts as a negative regulator of *sox9a*, *sox9b*, and *runx2b* in chondrocytes, perhaps through modulation of FGF signaling, and that *uxs1* function is required to turn on *runx2a* and *runx2b* in the perichondrium.

uxs1 mutants and Hedgehog signaling

Aberrant Hedgehog (Hh) signaling could explain many aspects of the described skeletal phenotype in *uxs1* mutants because Hh signaling drives proper histogenesis and morphogenesis of cartilage and perichondrium during endochondral ossification (Colnot et al., 2005; Cortes et al., 2009; Kronenberg, 2003; St-Jacques et al., 1999). In addition, proteoglycans are important for growth factor signaling, including that of the Hh family (Koziel et al., 2004; Lin, 2004). In normal development, *Indian hedgehog* (*Ihh*) is expressed in maturing chondrocytes, while expression of Patched (Ptc), a Hh receptor and target of Hh signaling, is restricted to proliferating chondrocytes and perichondrium (Avaron et al., 2006; Iwasaki et al., 1997; Nakase et al., 2001; Nakashima and de Crombrugghe, 2003; St-Jacques et al., 1999; Vortkamp et al., 1996). In wild-type ceratohyals at 5 dpf, *ihha* and *ihhb* were expressed in maturing chondrocytes located at the mid-diaphyseal region (Fig. 9A and C). In homozygous *uxs1* mutants, expression of *ihha* and *ihhb* was detected in chondrocytes of the ceratohyal, although it was unclear whether the overall expression pattern within the skeletal element was normal, due to the disrupted organization of the mutant cartilage (Fig. 9B and D). Similar patterns were observed at 4 and 6 dpf (data not shown). Given *ihh* expression in mutant cartilages, we next assayed for evidence of Hh signaling, which should be apparent in the expression of *ptc1* and *ptc2* (Goodrich et al., 1996; Lewis et al., 1999). In wild-type 5 dpf ceratohyals, *ptc1* and *ptc2* expression was relatively high in perichondrium and low in chondrocytes (Fig. 9E and G). Homozygous

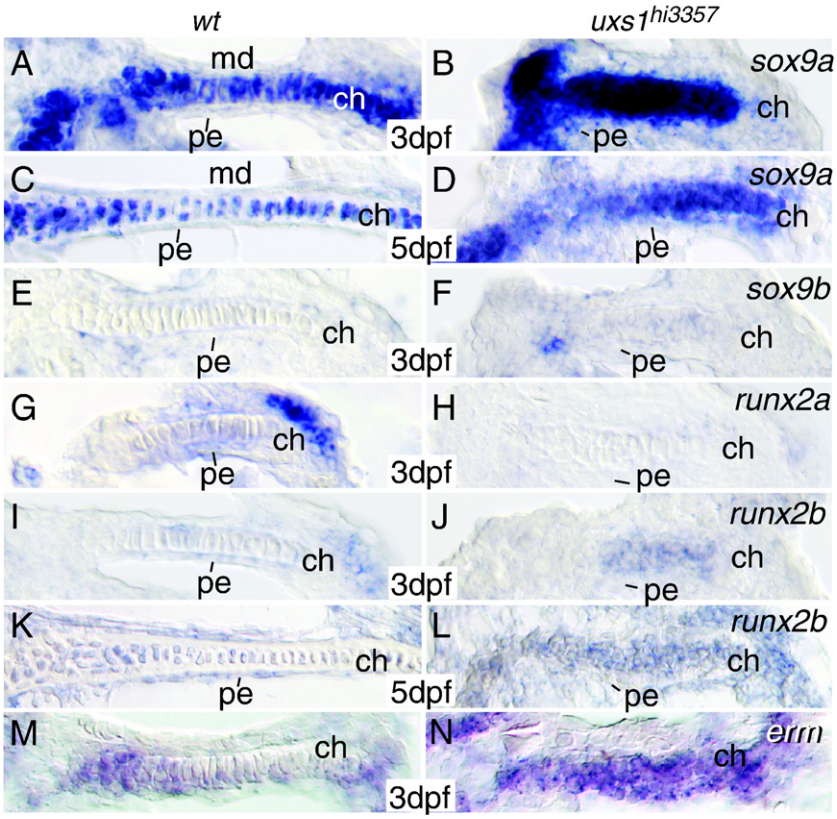

Fig. 8. Detection of molecular regulators of skeletogenesis in *uxs1* mutant cartilage. (A–N) *In situ* hybridization on horizontal sections through the ceratohyal for *sox9a* (A–D), *sox9b* (E, F), *runx2a* (G, H), *runx2b* (I–L), and *erm* (M, N). Wild-type chondrocytes in the mid-diaphyseal region showed decreased *sox9a* expression from 3 dpf (A) to 5 dpf (C) as they matured. Not only did chondrocytes of *uxs1*^{hi3357} mutants fail to show this down-regulation over time (B, D), but in addition, *sox9a* expression overall was much higher in mutants compared to wild types. Expression of *sox9b* was absent in wild-type chondrocytes at 3 dpf (E), but transcripts were detected in *uxs1* mutants (F). *runx2a* expression was obvious in perichondrium of wild types at 3 dpf (G), but was absent in *uxs1* mutants (H). *runx2b* expression was found in perichondrium of wild types at 3 dpf (I) and 5 dpf (K), but was not easily detected in perichondrium of mutants at these timepoints (J, L). In addition, chondrocyte expression of *runx2b* was much higher in *uxs1* mutants compared to wild types at 3 and 5 dpf. Expression of the FGF-responsive gene *erm* was found in just a few wild-type chondrocytes at 3 dpf (M), whereas *erm* transcripts were at high levels in all *uxs1* mutant chondrocytes (N). Abbreviations: ch, ceratohyal; md, mid-diaphyseal region; pe, perichondrium.

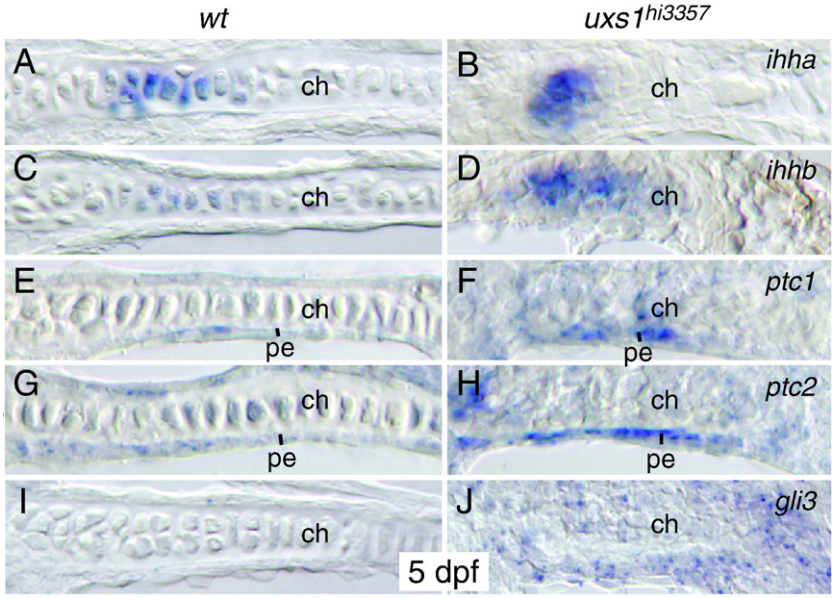

Fig. 9. Markers of Hedgehog signaling during *uxs1* mutant endochondral ossification. (A–J) *In situ* hybridization on horizontal sections through 5 dpf ceratohyal for *ihha* (A, B), *ihhb* (C, D), *ptc1* (E, F), *ptc2* (G, H), and *gli3* (I, J). Wild-type expression of *ihha* (A) and *ihhb* (B) appeared similar to that observed in *uxs1*^{hi3357} mutant chondrocytes (B, D). Compared to wild-type perichondrium (E, G, I), *uxs1* mutant perichondrium demonstrated increased expression of *ptc1* (F), *ptc2* (H), and *gli3* (J).

uxs1 mutants showed low levels of chondrocyte staining with the *ptc1* and *ptc2* probes, but expression in the perichondrium and surrounding tissues appeared to be up-regulated compared to wild types (Fig. 9F and H). Additional markers of Hh signaling, such as *gli1, gli2, gli3* and *pthrp1 and pthrp2* genes (Katoh and Katoh, 2009), were analyzed. Most of these genes showed weak expression in cartilage or perichondrium at this timepoint in both wild-type and mutant ceratohyals (data not shown), although *gli3* transcripts were at slightly higher levels in cells surrounding *uxs1* mutant cartilage than those observed in wild-type siblings (Fig. 9I and J). From these data, we conclude that Hedgehog signaling appeared to be functional and elevated during endochondral ossification in *uxs1* mutants, suggesting that normal Uxs1 activity inhibits Hh signaling.

Discussion

A unique model for analysis of Uxs1 function in vertebrates

Uxs1 is required for many functions of proteoglycans because this enzyme converts UDP-glucuronic acid to UDP-xylose, which is the initial sugar added to the core protein of many proteoglycans (Bar-Peled et al., 2001). Our phylogenetic analyses revealed Uxs1 to be one of the most broadly and strongly conserved non-mitochondrial proteins, with 57% amino acid identity shared between the bacterial and human enzymes. Despite its central biological importance, however, mutational analysis of Uxs1 function has been limited to three experimental systems, only one of which is a multicellular organism. A mutant pathogenic fungus *C. neoformans* shows that Uxs1 is required for fungal virulence through its action in biosynthesis of the capsule (Moyrand et al., 2002). Also, a Chinese hamster ovary *Uxs1*-mutant cell line (*pgsI-208*) was recently identified, providing insight into subcellular trafficking of UDP-xylose (Bakker et al., 2009). Finally, the *sqv-1* mutants of *C. elegans* demonstrate the requirement of Uxs1 in vulval morphogenesis and early zygotic cytokinesis (Hwang and Horvitz, 2002). With respect to vertebrates, however, zebrafish mutants offer both to reveal unique Uxs1 functions during skeletal histogenesis and morphogenesis, and to elucidate novel roles for proteoglycans.

We report here the functional consequences of two mutant alleles in zebrafish *uxs1*. The zebrafish mutation *hi3357* contains an insertion into a gene with reciprocal best BLAST relationship to human *UXS1* (Golling et al., 2002; Nissen et al., 2006), and the *mow*^{w60} mutation revealed a single disruptive nucleotide substitution in *uxs1* that changes an arginine to a histidine (R233H) in the Uxs1 protein. Arginine at this position has been conserved in all sequenced multicellular eukaryotes (plants, fungi, animals) for at least 1.6 billion years (Wang et al., 1999), as would be expected if it were important for enzymatic function. To determine whether the R233H mutation alters Uxs1 function, we introduced the same sequence change into the human *UXS1* gene and found that it abolished enzymatic activity. Similar to *uxs1*^{hi3357}, which disrupts exon 1 and decreases transcript stability or abundance, we conclude that *mow*^{w60} is a null activity allele. Modeling the *mow*^{w60} mutation with the crystal structure of human UXS1, we found that histidine cannot satisfy the salt-bridge with Glu230 or participate in the hydrogen bonding network supported by Arg233, both of which would introduce destabilizing contacts in the well-packed dimer interface and can explain the observed loss of enzyme activity.

Uxs1 function is essential for normal proteoglycan deposition

With insufficient UDP-xylose, proteoglycan synthesis should diminish, leading to defective extracellular matrix. Our results show that in the absence of Uxs1 function, negatively charged acidic mucopolysaccharides (Scott, 1996) and proteoglycans do not accumulate normally in the extracellular matrix of embryonic cartilages. We observed loss of Alcian blue staining for sulfated glycosaminoglycans, disruption of WGA staining for N-acetylglucosamine, a sugar in the GAG chains of cartilage proteoglycans (Lang et al., 2006), and absence of immunoreactivity to both heparan sulfate proteoglycans (HSPG), a major proteoglycan of many cell types, including skeletal cells, and chondroitin sulfate proteoglycans (CSPGs), the most abundant cartilage proteoglycan. The small amount of WGA staining we observed in *uxs1* mutants is likely either due to the synthesis of the proteoglycan keratan sulfate, which does not use UDP-xylose as a sugar linker (Knudson and Knudson, 2001), or due to Uxs1 protein, *uxs1* transcript, and/or UDP-xylose deposited maternally.

Uxs1 drives skeletal morphogenesis

Our histological stains and visualization of GFP-labeled cells revealed that Uxs1 function is required for normal morphogenesis of cartilage, perichondrium, and bone. Because prechondrogenic condensations appear on schedule and in correct anatomical locations in *uxs1* mutants, zygotic expression of *uxs1* is not essential for the migration of neural crest cells or for the condensation of the resulting mesenchyme into pre-cartilage elements. When wild-type embryos secrete large quantities of ECM, however, *uxs1* mutants begin to display dramatic morphological deficits in both cartilage and perichondrium. Chondrocytes of *uxs1* mutants persist as small, rounded cells and fail to intercalate and stack. Because both of these cell movements appear to be required for overall cartilage morphogenesis (Kimmel et al., 1998), *uxs1* mutants produce shorter, thicker cartilage elements. In the context that zygotic expression of *uxs1* is necessary for proper morphogenetic behaviors of chondrocytes, it is significant that mutant embryos have concomitant defects in morphogenesis of perichondral cells. This developmental coincidence may reflect a common origin for precursors of these two cell populations (Verreijdt et al., 2002) or may illustrate another dimension of the well-documented communication between chondrocytes and perichondrium (Karsenty and Wagner, 2002).

Disruption of normal domains of *col10a1* expression and Alizarin red staining in *uxs1* mutants shows that Uxs1 activity is required for normal bone formation along both endochondral and intramembranous pathways. While perichondral dysmorphogenesis can explain bone malformation along the endochondral pathway, our data demonstrate that proper growth of bones forming by the intramembranous pathway, such as the dentary, also requires Uxs1 function. While intramembranous ossification employs proteoglycans, other mutants in the proteoglycan synthesis pathway (discussed below) do not show a strong phenotype in this class of bones. Perhaps these genetic models have no obvious dermal bone phenotype because they do not affect both heparan and chondroitin sulfate production simultaneously (discussed below), as occurs in *uxs1* mutants. More generally, the fact that morphological defects in cartilage, perichondrium, and bone of *uxs1* mutants become apparent at the time that skeletogenic cells are secreting abundant ECM suggests that Uxs1-dependent components of the extracellular matrix play a significant role in complex morphogenetic processes. These effects may be mediated either directly by changing the extracellular environment upon which morphogenetic movements may rely or indirectly by proteoglycan influence on growth factor signaling.

Other vertebrate proteoglycan synthesis mutants

In the pathway of GAG biosynthesis, the substrate of Uxs1 (i.e., UDP-glucuronic acid) is the product of UDP-glucose dehydrogenase (Ugdh). In zebrafish, disruption of *ugdh* by mutation (*jekyll*) or antisense knockdown causes a decrease in Alcian blue staining in the pharyngeal cartilages that is less severe than that of *uxs1* (Busch-Nentwich et al., 2004; Neuhauss et al., 1996; Walsh and Stainier, 2001). If *ugdh*^{jekyll} were a null allele, it would be expected to have a phenotypic effect as strong as that of *uxs1*. Thus, the *ugdh*^{jekyll} Ile331-to-Asp substitution, which

occupies a nonpolar pocket of the enzyme (Walsh and Stainier, 2001), is likely to be either a hypomorph or zebrafish has mechanisms other than Ugdh to supply UDP-glucuronic acid.

Mutations in genes that encode enzymes downstream of Uxs1 in GAG synthesis also display disrupted skeletogenesis. Exostosins (Ext's) attach GAG sugars to growing proteoglycan chains. Full loss of function mutants for Ext1 and Ext2 in mouse is early embryonic lethal, precluding skeletal analyses. However, mouse models of heterozygous Ext loss of function have defects in skeletal homeostasis and development (Clement et al., 2008; Lin et al., 2000; Stickens et al., 2005). Additionally, numerous recent studies illustrate the importance of GAG sulfation in proper skeletal development. For example, Slc35b2 (formerly called Papst1) is necessary for GAG sulfation. Zebrafish mutations in *ext2, extl3,* and *slc35b2* result in embryos with short, wide pharyngeal skeletal elements exhibiting Alcian blue staining similar to, but generally less severe than, those of *uxs1* mutants (Clement et al., 2008; Karlstrom et al., 1996; Lee et al., 2004; Schilling et al., 1996). Where examined, these mutants also show reduced bone formation and aberrant bone morphogenesis, including perichondral bone. While the perichondrium appeared to be unaffected morphologically in *ext2* and *slc35b2* mutant zebrafish, our visualization of GFP-labeled cells in *uxs1* mutants clearly reveals morphological defects in formation of the perichondrium, offering a new model system in which to study molecular mechanisms of perichondral development. The similarities of *ugdh*, *uxs1*, *ext2*, and *extl3* mutants indicate that the proteoglycan biosynthetic pathway is necessary for proper histogenesis and morphogenesis of craniofacial cartilage and bone in zebrafish, but that the *uxs1* mutations described here have the most severe phenotypes. In the mouse, numerous genes in the sulfation pathway of CSPGs have been demonstrated to be important for proper ECM production in developing cartilage. Mutations in *Jaws* (Sohaskey et al., 2008), *Gpapp* (Frederick et al., 2008), and *Papss2* (Cortes et al., 2009) all result in chondrodysplasias, and are characterized specifically by under-sulfated CSPGs.

A novel role for proteoglycans during cartilage histogenesis

We hypothesize that defects in skeletal histogenesis, revealed from transcriptional profiles of such genes as *col2a1a* and *col10a1* in *uxs1* mutant cartilages, can be explained molecularly by Uxs1-dependent changes to Sox9 and Runx2 activity. Up-regulation of *col2a1a* in developing mutant chondrocytes was associated with increased transcript levels of *sox9a* and *sox9b*. These data can be explained by the fact that Sox9 regulates *Col2a1* transcription in tetrapods and teleosts (Lefebvre et al., 1997; Yan et al., 2002; Yan et al., 2005). On the other hand, *uxs1* mutant chondrocytes failed to express the maturation marker *col10a1* on the appropriate timetable, even though *runx2b* was up-regulated in these cells. Since Runx2 is a transcriptional activator of *Col10a1* expression in tetrapods (Iwamoto et al., 2003; Komori, 2005; Yoshida et al., 2004; Zheng et al., 2003), perhaps a repressor of Runx2 protein activity is present in mutant chondrocytes. Indeed, over-expression of Sox9 in chondrocytes undergoing endochondral ossification abolishes *Col10a1* expression (Eames et al., 2004), and Sox9 protein inhibits activity of Runx2 through a direct molecular interaction (Zhou et al., 2006). Therefore, elevated expression of *sox9a* and *sox9b* in mutant chondrocytes may obviate the effects of increased *runx2b* levels, assuming the *sox9* mRNAs are translated to increased protein levels in *uxs1* mutant chondrocytes. We conclude that the molecular mechanism by which histogenic programs are altered in *uxs1* mutant chondrocytes is mediated, at least in part, through aberrant regulation of Sox9 levels and/or activity.

Why is *sox9* gene expression increased in *uxs1*-deficient chondrogenic cells? If Uxs1 promotes differentiation of *sox9*-expressing prechondrocytes, then in the absence of Uxs1 function, these cells would arrest and accumulate, effectively increasing *sox9* expression. However, our analyses of transgenic animals revealed no dramatic changes to the number of cells in a pre-cartilage element. Our developmental time series suggests a novel role for proteoglycans during cartilage histogenesis: they feed back onto expression of chondrogenic genes, such as *sox9*. Up-regulation of *sox9* only occurred after chondrogenic cells began to secrete abundant proteoglycans, as detected by antibodies to chondroitin sulfate, at 3 dpf. Levels of *sox9* transcripts were similar between wild type and *uxs1* mutant chondrogenic condensations at 48 hpf, for example (data not shown). Therefore, either proteoglycan-dependent cell signaling (discussed below), or some other integrin-like mechanism by which cells directly sense proteoglycans in the ECM, may normally repress *sox9* expression during early stages of chondrocyte differentiation (Fig. 10). While the answer to this interesting cell biological question remains unclear, other zebrafish mutants of proteoglycan synthesis and secretion show similarly increased *sox9a* levels in differentiating chondrocytes

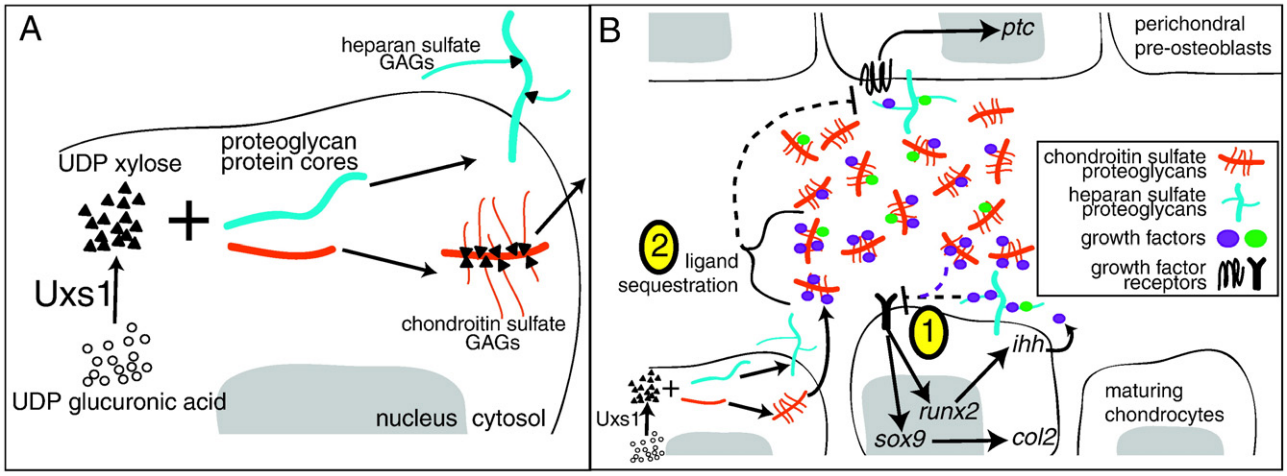

Fig. 10. The role of Uxs1 and the extracellular matrix in skeletogenesis. (A) Uxs1 converts UDP-glucuronic acid (open circles) to UDP-xylose (closed triangles), which serves as the linker sugar between the protein core (thick red and blue lines) and subsequent glycosaminoglycan deposition (thin red and blue lines) for heparan sulfate and chondroitin sulfate proteoglycans. Endoplasmic reticulum and secretory organelles are omitted for simplicity. (B) Model for signaling roles of proteoglycans as they mediate interactions between chondrocytes and perichondrium during endochondral ossification. (1) Throughout chondrocyte development, proteoglycans negatively regulate growth factor signaling, such as FGF, that serves to promote *sox9* expression, which would otherwise drive *col2* transcription. In a similar fashion in maturing chondrocytes, proteoglycans inhibit *runx2* expression, which would otherwise drive expression of markers of chondrocyte maturation, such as *ihh*. (2) When Ihh is produced by maturing chondrocytes, proteoglycans negatively regulate its action on perichondral pre-osteoblasts by ligand sequestration.

(Clement et al., 2008; Lang et al., 2006), suggesting a novel feedback mechanism from ECM during early stages of chondrogenesis.

Alterations to cell signaling in uxs1 mutants

In *Drosophila* and vertebrates, proteoglycans can act as co-receptors in signal transduction pathways (Iozzo, 1998; Lin, 2004; Lin et al., 1999). We hypothesize that disruption of the ECM, as shown by the aberrant distribution of Col2a1, *N*-acetylglucosamine, CSPG, and HSPG in *uxs1* mutants, leads to abnormal proteoglycan-facilitated developmental signaling between chondrocytes and perichondrium (Goldring et al., 2006; Olsen et al., 2000; Provot and Schipani, 2005). HSPGs, for example, modify Hedgehog (Hh) signaling, which is an important mediator between chondrocytes and perichondral cells during development (Colnot et al., 2005; Cortes et al., 2009; Kronenberg, 2003; St-Jacques et al., 1999). In *Drosophila*, the HSPG protein core mutant *dlp* is required for proper Hh signaling (Lum et al., 2003). Also, HSPGs may act as co-factors of ADAM-dependent release and spread of Shh (Dierker et al., 2009). On the other hand, our finding that *ptc* genes are up-regulated in the perichondrium of *uxs1* mutants is in agreement with vertebrate studies of proteoglycan synthesis mutants. For example, *Ext1* mutant mice show increased Ihh activity and range of Ihh signaling (Hilton et al., 2005; Koziel et al., 2004). These data inform a model whereby proteoglycans inhibit intensity and range of Hh signaling, perhaps by ligand sequestration (Fig. 10). On the other hand, under-sulfation of CSPGs decreased the range of Ihh diffusion within cartilage matrix (Cortes et al, 2009). In this light, proteoglycans may exert different effects on short-range signaling of Ihh to perichondral cells versus long-range Ihh signaling to periarticular chondrocytes. In fact, these differences may reflect reliance upon HSPG- versus CSPG-mediated Hh signaling.

Many of the defects described here in *uxs1* skeletogenesis can be explained by proteoglycan-dependent alterations to growth factor signaling as chondrogenic cells embed themselves in abundant ECM. HSPGs promote a functional signaling complex between Fibroblast growth factors (FGFs) and their receptors (FGFRs) (Ornitz, 2000; Pellegrini, 2001) and HSPG sulfation is required for the interaction of FGFs with their receptors (Nakato and Kimata, 2002). *Fgfr2* is expressed in chondrogenic condensations, and FGF signaling functions upstream of *Sox9* during chondrogenesis (Coumoul and Deng, 2003; de Crombrugghe et al., 2000; Eames and Schneider, 2008; Itoh and Ornitz, 2004; Ornitz and Itoh, 2001). Interestingly, we found increased expression of the FGF-responsive gene *erm* in chondrocytes of *uxs1* mutants, suggesting that cartilage proteoglycans, such as CSPGs, may normally inhibit FGF signaling. Taken together, proteoglycan-dependent alterations to FGF signaling may explain our finding that *sox9a* and *sox9b* are up-regulated in *uxs1* mutant chondrocytes (Fig. 10).

uxs1 and disease

Besides the role of *uxs1* in skeletogenesis, defects in proteoglycan-mediated pathways can disrupt other aspects of human health. Chondroitin sulfate proteoglycan helps protect neurons against the buildup of β-amyloid protein, an indicator of Alzheimer's disease progression (Miyata et al., 2007). Proteoglycans are important for tumorigenesis, and the blocking of heparan sulfate synthesis may inhibit metastasis (Belting et al., 2002). Given the central role of UDP-xylose in proteoglycan biosynthesis, the *mow*^{w60} zebrafish that we report here is the first thoroughly investigated animal model deficient in *uxs1*, and will be a useful tool for studying the role of proteoglycans in health and disease.

Acknowledgments

Thanks to Ruth Bremiller and Amanda Rapp for assistance with histology and animal care, and to Jeremy Wegner and Yasuko Honjo for *erm*, *gli1*, *gli2*, and *gli3* probes. G.A.S. submitted a portion of this work as an undergraduate thesis to the Clark Honors College, University of Oregon, and offers special thanks to Nathan Tublitz and Joseph Fracchia. B.F.E. would like to thank Charles Kimmel for his support. This work was supported by grant numbers 5 F32 DE016778-03 (B.F.E.), R01 DE13834 (C.B.K.), and 5R01RR020833 and P01 HD22486 (J.H.P.) from the National Institutes of Health. The contents of this study are solely the responsibility of the authors and do not necessarily represent the official views of NCRR or NIH.

References

Akiyama, H., 2008. Control of chondrogenesis by the transcription factor Sox9. Mod. Rheumatol. 18, 213–219.
Ala-Kokko, L., Baldwin, C.T., Moskowitz, R.W., Prockop, D.J., 1990. Single base mutation in the type II procollagen gene (COL2A1) as a cause of primary osteoarthritis associated with a mild chondrodysplasia. Proc. Natl. Acad. Sci. U. S. A. 87, 6565–6568.
Amsterdam, A., Nissen, R.M., Sun, Z., Swindell, E.C., Farrington, S., Hopkins, N., 2004. Identification of 315 genes essential for early zebrafish development. Proc. Natl. Acad. Sci. U. S. A. 101, 12792–12797.
Avaron, F., Hoffman, L., Guay, D., Akimenko, M.A., 2006. Characterization of two new zebrafish members of the hedgehog family: atypical expression of a zebrafish indian hedgehog gene in skeletal elements of both endochondral and dermal origins. Dev. Dyn. 235, 478–489.
Bakker, H., Oka, T., Ashikov, A., Yadav, A., Berger, M., Rana, N.A., Bai, X., Jigami, Y., Haltiwanger, R.S., Esko, J.D., Gerardy-Schahn, R., 2009. Functional UDP-xylose transport across the endoplasmic reticulum/Golgi membrane in a Chinese hamster ovary cell mutant defective in UDP-xylose Synthase. J. Biol. Chem. 284, 2576–2583.
Bar-Peled, M., Griffith, C.L., Doering, T.L., 2001. Functional cloning and characterization of a UDP- glucuronic acid decarboxylase: the pathogenic fungus *Cryptococcus neoformans* elucidates UDP-xylose synthesis. Proc. Natl. Acad. Sci. U. S. A. 98, 12003–12008.
Belting, M., Borsig, L., Fuster, M.M., Brown, J.R., Persson, L., Fransson, L.A., Esko, J.D., 2002. Tumor attenuation by combined heparan sulfate and polyamine depletion. Proc. Natl. Acad. Sci. U. S. A. 99, 371–376.
Birney, E., Andrews, T.D., Bevan, P., Caccamo, M., Chen, Y., Clarke, L., Coates, G., Cuff, J., Curwen, V., Cutts, T., Down, T., Eyras, E., Fernandez-Suarez, X.M., Gane, P., Gibbins, B., Gilbert, J., Hammond, M., Hotz, H.R., Iyer, V., Jekosch, K., Kahari, A., Kasprzyk, A., Keefe, D., Keenan, S., Lehvaslaiho, H., McVicker, G., Melsopp, C., Meidl, P., Mongin, E., Pettett, R., Potter, S., Proctor, G., Rae, M., Searle, S., Slater, G., Smedley, D., Smith, J., Spooner, W., Stabenau, A., Stalker, J., Storey, R., Ureta-Vidal, A., Woodwark, K.C., Cameron, G., Durbin, R., Cox, A., Hubbard, T., Clamp, M., 2004. An overview of Ensembl. Genome Res. 14, 925–928.
Busch-Nentwich, E., Sollner, C., Roehl, H., Nicolson, T., 2004. The deafness gene dfna5 is crucial for ugdh expression and HA production in the developing ear in zebrafish. Development 131, 943–951.
Clement, A., Wiweger, M., von der Hardt, S., Rusch, M.A., Selleck, S.B., Chien, C.B., Roehl, H.H., 2008. Regulation of zebrafish skeletogenesis by ext2/dackel and papst1/pinscher. PLoS Genet. 4, e1000136.
Colnot, C., de la Fuente, L., Huang, S., Hu, D., Lu, C., St-Jacques, B., Helms, J.A., 2005. Indian hedgehog synchronizes skeletal angiogenesis and perichondrial maturation with cartilage development. Development 132, 1057–1067.
Cortes, M., Baria, A.T., Schwartz, N.B., 2009. Sulfation of chondroitin sulfate proteoglycans is necessary for proper Indian hedgehog signaling in the developing growth plate. Development 136, 1697–1706.
Coumoul, X., Deng, C.X., 2003. Roles of FGF receptors in mammalian development and congenital diseases. Birth Defects Res. C Embryo Today 69, 286–304.
Cubbage, C.C., Mabee, P.M., 1996. Development of the Cranium and Paird Fins in the Zebrafish *Danio rerio* (Ostariophysi, Cyprinidae). J. Morphol. 229, 121–160.
Dao-pin, S., Anderson, D.E., Baase, W.A., Dahlquist, F.W., Matthews, B.W., 1991. Structural and thermodynamic consequences of burying a charged residue within the hydrophobic core of T4 lysozyme. Biochemistry 30, 11521–11529.
de Crombrugghe, B., Lefebvre, V., Behringer, R.R., Bi, W., Murakami, S., Huang, W., 2000. Transcriptional mechanisms of chondrocyte differentiation. Matrix Biol. 19, 389–394.
DeLano, W.L., 2002. The PyMOL User's Manual. DeLano Scientific, Palo Alto, CA, USA.
Dierker, T., Dreier, R., Petersen, A., Bordych, C., Grobe, K., 2009. Heparan sulfate-modulated, metalloprotease-mediated sonic hedgehog release from producing cells. J. Biol. Chem. 284, 8013–8022.
Eames, B.F., Helms, J.A., 2004. Conserved molecular program regulating cranial and appendicular skeletogenesis. Dev. Dyn. 231, 4–13.
Eames, B.F., Schneider, R.A., 2008. The genesis of cartilage size and shape during development and evolution. Development 135, 3947–3958.
Eames, B.F., de la Fuente, L., Helms, J.A., 2003. Molecular ontogeny of the skeleton. Birth Defects Res. C Embryo Today 69, 93–101.
Eames, B.F., Sharpe, P.T., Helms, J.A., 2004. Hierarchy revealed in the specification of three skeletal fates by Sox9 and Runx2. Dev. Biol. 274, 188–200.
Frederick, J.P., Tafari, A.T., Wu, S.M., Megosh, L.C., Chiou, S.T., Irving, R.P., York, J.D., 2008. A role for a lithium-inhibited Golgi nucleotidase in skeletal development and sulfation. Proc. Natl. Acad. Sci. U. S. A. 105, 11605–11612.
Goldring, M.B., Tsuchimochi, K., Ijiri, K., 2006. The control of chondrogenesis. J. Cell. Biochem. 97, 33–44.
Golling, G., Amsterdam, A., Sun, Z., Antonelli, M., Maldonado, E., Chen, W., Burgess, S., Haldi, M., Artzt, K., Farrington, S., Lin, S.Y., Nissen, R.M., Hopkins, N., 2002.

Insertional mutagenesis in zebrafish rapidly identifies genes essential for early vertebrate development. Nat. Genet. 31, 135–140.
Goodrich, L.V., Johnson, R.L., Milenkovic, L., McMahon, J.A., Scott, M.P., 1996. Conservation of the hedgehog/patched signaling pathway from flies to mice: induction of a mouse patched gene by Hedgehog. Genes Dev. 10, 301–312.
Hamerman, D., 1989. The biology of osteoarthritis. N. Engl. J. Med. 320, 1322–1330.
Hedges, S.B., 2002. The origin and evolution of model organisms. Nat. Rev. Genet. 3, 838–849.
Henikoff, S., Henikoff, J.G., 1992. Amino acid substitution matrices from protein blocks. Proc. Natl. Acad. Sci. U. S. A. 89, 10915–10919.
Hilton, M.J., Gutierrez, L., Martinez, D.A., Wells, D.E., 2005. EXT1 regulates chondrocyte proliferation and differentiation during endochondral bone development. Bone 36, 379–386.
Holt, C.E., Dickson, B.J., 2005. Sugar codes for axons? Neuron 46, 169–172.
Hwang, H.Y., Horvitz, H.R., 2002. The SQV-1 UDP-glucuronic acid decarboxylase and the SQV-7 nucleotide-sugar transporter may act in the Golgi apparatus to affect Caenorhabditis elegans vulval morphogenesis and embryonic development. Proc. Natl. Acad. Sci. USA. 99, 14218–14223.
Iozzo, R.V., 1998. Matrix proteoglycans: from molecular design to cellular function. Annu. Rev. Biochem. 67, 609–652.
Ishimizu, T., Sano, K., Uchida, T., Teshima, H., Omichi, K., Hojo, H., Nakahara, Y., Hase, S., 2007. Purification and substrate specificity of UDP-D-xylose:beta-D-glucoside alpha-1, 3-D-xylosyltransferase involved in the biosynthesis of the Xyl alpha1–3Xyl alpha1–3Glc beta1-*O*-Ser on epidermal growth factor-like domains. J. Biochem. 141, 593–600.
Itoh, N., Ornitz, D.M., 2004. Evolution of the Fgf and Fgfr gene families. Trends Genet. 20, 563–569.
Iwamoto, M., Kitagaki, J., Tamamura, Y., Gentili, C., Koyama, E., Enomoto, H., Komori, T., Pacifici, M., Enomoto-Iwamoto, M., 2003. Runx2 expression and action in chondrocytes are regulated by retinoid signaling and parathyroid hormone-related peptide (PTHrP). Osteoarthritis Cartilage 11, 6–15.
Iwasaki, M., Le, A.X., Helms, J.A., 1997. Expression of indian hedgehog, bone morphogenetic protein 6 and gli during skeletal morphogenesis. Mech. Dev. 69, 197–202.
Izvolsky, K.I., Shoykhet, D., Yang, Y., Yu, Q., Nugent, M.A., Cardoso, W.V., 2003. Heparan sulfate-FGF10 interactions during lung morphogenesis. Dev. Biol. 258, 185–200.
Jowett, T., Yan, Y.L., 1996. Double fluorescent in situ hybridization to zebrafish embryos. Trends Genet. 12, 387–389.
Karlstrom, R.O., Trowe, T., Klostermann, S., Baier, H., Brand, M., Crawford, A.D., Grunewald, B., Haffter, P., Hoffmann, H., Meyer, S.U., Muller, B.K., Richter, S., van Eeden, F.J., Nusslein-Volhard, C., Bonhoeffer, F., 1996. Zebrafish mutations affecting retinotectal axon pathfinding. Development 123, 427–438.
Karsenty, G., Wagner, E.F., 2002. Reaching a genetic and molecular understanding of skeletal development. Dev. Cell. 2, 389–406.
Kasprzyk, A., Keefe, D., Smedley, D., London, D., Spooner, W., Melsopp, C., Hammond, M., Rocca-Serra, P., Cox, T., Birney, E., 2004. EnsMart: a generic system for fast and flexible access to biological data. Genome Res. 14, 160–169.
Katoh, Y., Katoh, M., 2009. Hedgehog target genes: mechanisms of carcinogenesis induced by aberrant hedgehog signaling activation. Curr. Mol. Med. 9, 873–886.
Kearns, A.E., Vertel, B.M., Schwartz, N.B., 1993. Topography of glycosylation and UDP-xylose production. J. Biol. Chem. 268, 11097–11104.
Kimmel, C.B., Miller, C.T., Kruze, G., Ullmann, B., BreMiller, R.A., Larison, K.D., Snyder, H.C., 1998. The shaping of pharyngeal cartilages during early development of the zebrafish. Dev. Biol. 203, 245–263.
Kirn-Safran, C.B., Gomes, R.R., Brown, A.J., Carson, D.D., 2004. Heparan sulfate proteoglycans: coordinators of multiple signaling pathways during chondrogenesis. Birth Defects Res. C Embryo Today 72, 69–88.
Kizawa, H., Kou, I., Iida, A., Sudo, A., Miyamoto, Y., Fukuda, A., Mabuchi, A., Kotani, A., Kawakami, A., Yamamoto, S., Uchida, A., Nakamura, K., Notoya, K., Nakamura, Y., Ikegawa, S., 2005. An aspartic acid repeat polymorphism in asporin inhibits chondrogenesis and increases susceptibility to osteoarthritis. Nat. Genet. 37, 138–144.
Kjellen, L., Lindahl, U., 1991. Proteoglycans: structures and interactions. Annu. Rev. Biochem. 60, 443–475.
Knapik, E.W., Goodman, A., Ekker, M., Chevrette, M., Delgado, J., Neuhauss, S., Shimoda, N., Driever, W., Fishman, M.C., Jacob, H.J., 1998. A microsatellite genetic linkage map for zebrafish (*Danio rerio*). Nat. Genet. 18, 338–343.
Knowlton, R.G., Katzenstein, P.L., Moskowitz, R.W., Weaver, E.J., Malemud, C.J., Pathria, M.N., Jimenez, S.A., Prockop, D.J., 1990. Genetic linkage of a polymorphism in the type II procollagen gene (COL2A1) to primary osteoarthritis associated with mild chondrodysplasia. N. Engl. J. Med. 322, 526–530.
Knudson, C.B., Knudson, W., 2001. Cartilage proteoglycans. Semin. Cell Dev. Biol. 12, 69–78.
Komori, T., 2005. Regulation of skeletal development by the Runx family of transcription factors. J. Cell. Biochem. 95, 445–453.
Koziel, L., Kunath, M., Kelly, O.G., Vortkamp, A., 2004. Ext1-dependent heparan sulfate regulates the range of Ihh signaling during endochondral ossification. Dev. Cell 6, 801–813.
Kronenberg, H.M., 2003. Developmental regulation of the growth plate. Nature 423, 332–336.
Krovel, A.V., Olsen, L.C., 2004. Sexual dimorphic expression pattern of a splice variant of zebrafish vasa during gonadal development. Dev. Biol. 271, 190–197.
Lander, A.D., Selleck, S.B., 2000. The elusive functions of proteoglycans: in vivo veritas. J. Cell Biol. 148, 227–232.
Lang, M.R., Lapierre, L.A., Frotscher, M., Goldenring, J.R., Knapik, E.W., 2006. Secretory COPII coat component Sec23a is essential for craniofacial chondrocyte maturation. Nat. Genet. 38, 1198–1203.
Lawson, N.D., Weinstein, B.M., 2002. In vivo imaging of embryonic vascular development using transgenic zebrafish. Dev. Biol. 248, 307–318.
Lee, J.S., von der Hardt, S., Rusch, M.A., Stringer, S.E., Stickney, H.L., Talbot, W.S., Geisler, R., Nusslein-Volhard, C., Selleck, S.B., Chien, C.B., Roehl, H., 2004. Axon sorting in the optic tract requires HSPG synthesis by ext2 (dackel) and extl3 (boxer). Neuron 44, 947–960.
Lefebvre, V., Huang, W., Harley, V.R., Goodfellow, P.N., de Crombrugghe, B., 1997. SOX9 is a potent activator of the chondrocyte-specific enhancer of the pro alpha1(II) collagen gene. Mol. Cell. Biol. 17, 2336–2346.
Lewis, K.E., Concordet, J.P., Ingham, P.W., 1999. Characterisation of a second patched gene in the zebrafish *Danio rerio* and the differential response of patched genes to Hedgehog signalling. Dev. Biol. 208, 14–29.
Lin, X., 2004. Functions of heparan sulfate proteoglycans in cell signaling during development. Development 131, 6009–6021.
Lin, X., Buff, E.M., Perrimon, N., Michelson, A.M., 1999. Heparan sulfate proteoglycans are essential for FGF receptor signaling during *Drosophila* embryonic development. Development 126, 3715–3723.
Lin, X., Wei, G., Shi, Z., Dryer, L., Esko, J.D., Wells, D.E., Matzuk, M.M., 2000. Disruption of gastrulation and heparan sulfate biosynthesis in EXT1-deficient mice. Dev. Biol. 224, 299–311.
Lum, L., Yao, S., Mozer, B., Rovescalli, A., Von Kessler, D., Nirenberg, M., Beachy, P.A., 2003. Identification of Hedgehog pathway components by RNAi in *Drosophila* cultured cells. Science 299, 2039–2045.
Miyata, S., Nishimura, Y., Nakashima, T., 2007. Perineuronal nets protect against amyloid beta-protein neurotoxicity in cultured cortical neurons. Brain Res.
Moyrand, F., Klaproth, B., Himmelreich, U., Dromer, F., Janbon, G., 2002. Isolation and characterization of capsule structure mutant strains of *Cryptococcus neoformans*. Mol. Microbiol. 45, 837–849.
Nakase, T., Miyaji, T., Kuriyama, K., Tamai, N., Horiki, M., Tomita, T., Myoui, A., Shimada, K., Yoshikawa, H., 2001. Immunohistochemical detection of parathyroid hormone-related peptide, Indian hedgehog, and patched in the process of endochondral ossification in the human. Histochem. Cell Biol. 116, 277–284.
Nakashima, K., de Crombrugghe, B., 2003. Transcriptional mechanisms in osteoblast differentiation and bone formation. Trends Genet. 19, 458–466.
Nakato, H., Kimata, K., 2002. Heparan sulfate fine structure and specificity of proteoglycan functions. Biochim. Biophys. Acta 1573, 312–318.
Neuhauss, S.C., Solnica-Krezel, L., Schier, A.F., Zwartkruis, F., Stemple, D.L., Malicki, J., Abdelilah, S., Stainier, D.Y., Driever, W., 1996. Mutations affecting craniofacial development in zebrafish. Development 123, 357–367.
Nissen, R.M., Amsterdam, A., Hopkins, N., 2006. A zebrafish screen for craniofacial mutants identifies wdr68 as a highly conserved gene required for endothelin-1 expression. BMC Dev. Biol. 6, 28.
Olsen, B.R., Reginato, A.M., Wang, W., 2000. Bone development. Annu. Rev. Cell Dev. Biol. 16, 191–220.
Ornitz, D.M., 2000. FGFs, heparan sulfate and FGFRs: complex interactions essential for development. Bioessays 22, 108–112.
Ornitz, D.M., Itoh, N., 2001. Fibroblast growth factors. Genome Biol. 2 REVIEWS3005.
Otto, F., Thornell, A.P., Crompton, T., Denzel, A., Gilmour, K.C., Rosewell, I.R., Stamp, G.W., Beddington, R.S., Mundlos, S., Olsen, B.R., Selby, P.B., Owen, M.J., 1997. Cbfa1, a candidate gene for cleidocranial dysplasia syndrome, is essential for osteoblast differentiation and bone development. Cell 89, 765–771.
Pellegrini, L., 2001. Role of heparan sulfate in fibroblast growth factor signalling: a structural view. Curr. Opin. Struct. Biol. 11, 629–634.
Piotrowski, T., Schilling, T.F., Brand, M., Jiang, Y.J., Heisenberg, C.P., Beuchle, D., Grandel, H., van Eeden, F.J., Furutani-Seiki, M., Granato, M., Haffter, P., Hammerschmidt, M., Kane, D.A., Kelsh, R.N., Mullins, M.C., Odenthal, J., Warga, R.M., Nusslein-Volhard, C., 1996. Jaw and branchial arch mutants in zebrafish II: anterior arches and cartilage differentiation. Development 123, 345–356.
Provot, S., Schipani, E., 2005. Molecular mechanisms of endochondral bone development. Biochem. Biophys. Res. Commun. 328, 658–665.
Prydz, K., Dalen, K.T., 2000. Synthesis and sorting of proteoglycans. J. Cell Sci. 113 (Pt 2), 193–205.
Renn, J., Winkler, C., Schartl, M., Fischer, R., Goerlich, R., 2006. Zebrafish and medaka as models for bone research including implications regarding space-related issues. Protoplasma 229, 209–214.
Rothschild, B.M., Panza, R.K., 2007. Lack of bone stiffness/strength contribution to osteoarthritis—evidence for primary role of cartilage damage. Rheumatology (Oxford) 46, 246–249.
Schilling, T.F., Piotrowski, T., Grandel, H., Brand, M., Heisenberg, C.P., Jiang, Y.J., Beuchle, D., Hammerschmidt, M., Kane, D.A., Mullins, M.C., van Eeden, F.J., Kelsh, R.N., Furutani-Seiki, M., Granato, M., Haffter, P., Odenthal, J., Warga, R.M., Trowe, T., Nusslein-Volhard, C., 1996. Jaw and branchial arch mutants in zebrafish I: branchial arches. Development 123, 329–344.
Scott, J.E., 1996. Alcian blue. Now you see it, now you don't. Eur. J. Oral Sci. 104, 2–9.
Shimoda, N., Knapik, E.W., Ziniti, J., Sim, C., Yamada, E., Kaplan, S., Jackson, D., de Sauvage, F., Jacob, H., Fishman, M.C., 1999. Zebrafish genetic map with 2000 microsatellite markers. Genomics 58, 219–232.
Simoes, B., Conceicao, N., Viegas, C.S., Pinto, J.P., Gavaia, P.J., Hurst, L.D., Kelsh, R.N., Cancela, M.L., 2006. Identification of a promoter element within the zebrafish colXalpha1 gene responsive to runx2 isoforms Osf2/Cbfa1 and til-1 but not to pebp2alphaA2. Calcif. Tissue Int. 79, 230–244.
Sohaskey, M.L., Yu, J., Diaz, M.A., Plaas, A.H., Harland, R.M., 2008. JAWS coordinates chondrogenesis and synovial joint positioning. Development 135, 2215–2220.
Stickens, D., Zak, B.M., Rougier, N., Esko, J.D., Werb, Z., 2005. Mice deficient in Ext2 lack heparan sulfate and develop exostoses. Development 132, 5055–5068.
St-Jacques, B., Hammerschmidt, M., McMahon, A.P., 1999. Indian hedgehog signaling regulates proliferation and differentiation of chondrocytes and is essential for bone formation. Genes Dev. 13, 2072–2086.
van den Berg, S., Lofdahl, P.A., Hard, T., Berglund, H., 2006. Improved solubility of TEV protease by directed evolution. J. Biotechnol. 121, 291–298.

Velleman, S.G., 2000. The role of the extracellular matrix in skeletal development. Poult. Sci. 79, 985–989.
Velleman, S.G., Clark, S.H., 1992. The cartilage proteoglycan deficient mutation, nanomelia, contains a DNA polymorphism in the proteoglycan core protein gene that is genetically linked to the nanomelia phenotype. Matrix 12, 66–72.
Verreijdt, L., Vandervennet, E., Sire, J.Y., Huysseune, A., 2002. Developmental differences between cranial bones in the zebrafish (*Danio rerio*): some preliminary light and TEM observations. Connect. Tissue Res. 43, 109–112.
Vertel, B.M., Walters, L.M., Flay, N., Kearns, A.E., Schwartz, N.B., 1993. Xylosylation is an endoplasmic reticulum to Golgi event. J. Biol. Chem. 268, 11105–11112.
Vortkamp, A., Lee, K., Lanske, B., Segre, G.V., Kronenberg, H.M., Tabin, C.J., 1996. Regulation of rate of cartilage differentiation by Indian hedgehog and PTH-related protein. Science 273, 613–622.
Walker, M., Kimmel, C., 2007. A two-color acid-free cartilage and bone stain for zebrafish larvae. Biotech. Histochem. 82, 23–28.
Walsh, E.C., Stainier, D.Y., 2001. UDP-glucose dehydrogenase required for cardiac valve formation in zebrafish. Science 293, 1670–1673.
Wang, D.Y., Kumar, S., Hedges, S.B., 1999. Divergence time estimates for the early history of animal phyla and the origin of plants, animals and fungi. Proc. Biol. Sci. 266, 163–171.
Woods, I.G., Wilson, C., Friedlander, B., Chang, P., Reyes, D.K., Nix, R., Kelly, P.D., Chu, F., Postlethwait, J.H., Talbot, W.S., 2005. The zebrafish gene map defines ancestral vertebrate chromosomes. Genome Res. 15, 1307–1314.
Yan, Y.L., Hatta, K., Riggleman, B., Postlethwait, J.H., 1995. Expression of a type II collagen gene in the zebrafish embryonic axis. Dev. Dyn. 203, 363–376.
Yan, Y.L., Miller, C.T., Nissen, R.M., Singer, A., Liu, D., Kirn, A., Draper, B., Willoughby, J., Morcos, P.A., Amsterdam, A., Chung, B.C., Westerfield, M., Haffter, P., Hopkins, N., Kimmel, C., Postlethwait, J.H., 2002. A zebrafish sox9 gene required for cartilage morphogenesis. Development 129, 5065–5079.
Yan, Y.L., Willoughby, J., Liu, D., Crump, J.G., Wilson, C., Miller, C.T., Singer, A., Kimmel, C., Westerfield, M., Postlethwait, J.H., 2005. A pair of Sox: distinct and overlapping functions of zebrafish sox9 co-orthologs in craniofacial and pectoral fin development. Development 132, 1069–1083.
Yoshida, C.A., Komori, T., 2005. Role of Runx proteins in chondrogenesis. Crit. Rev. Eukaryot. Gene Expr. 15, 243–254.
Yoshida, C.A., Yamamoto, H., Fujita, T., Furuichi, T., Ito, K., Inoue, K., Yamana, K., Zanma, A., Takada, K., Ito, Y., Komori, T., 2004. Runx2 and Runx3 are essential for chondrocyte maturation, and Runx2 regulates limb growth through induction of Indian hedgehog. Genes Dev. 18, 952–963.
Zheng, Q., Zhou, G., Morello, R., Chen, Y., Garcia-Rojas, X., Lee, B., 2003. Type X collagen gene regulation by Runx2 contributes directly to its hypertrophic chondrocyte-specific expression in vivo. J. Cell Biol. 162, 833–842.
Zhou, G., Zheng, Q., Engin, F., Munivez, E., Chen, Y., Sebald, E., Krakow, D., Lee, B., 2006. Dominance of SOX9 function over RUNX2 during skeletogenesis. Proc. Natl. Acad. Sci. U. S. A. 103, 19004–19009.